



# Geochemistry of surface sediments from the fjords of Northern Chilean Patagonia (44–47°S): Spatial variability and implications for paleoclimate reconstructions

Sébastien Bertrand<sup>a,b,\*</sup>, Konrad A. Hughen<sup>a</sup>, Julio Sepúlveda<sup>c</sup>, Silvio Pantoja<sup>d</sup>

<sup>a</sup> Marine Chemistry and Geochemistry, Woods Hole Oceanographic Institution, 360 Woods Hole Road, Woods Hole, MA 02543, USA

<sup>b</sup> Renard Centre of Marine Geology, University of Ghent, Krijgslaan 281 s.8, 9000 Gent, Belgium

<sup>c</sup> Department of Earth, Atmospheric and Planetary Sciences, Massachusetts Institute of Technology, 45 Carleton Street, E25-623, Cambridge, MA 02139, USA

<sup>d</sup> Department of Oceanography, Center for Oceanographic Research in the Eastern South Pacific, and COPAS Sur-Austral, University of Concepción, P.O. Box 160-C, Concepción, Chile

Received 21 June 2011; accepted in revised form 17 October 2011; available online 20 October 2011

## Abstract

The Patagonian fjords have a clear potential to provide high-resolution sedimentary and geochemical records of past climate and environmental change in the Southern Andes. To improve our ability to interpret these proxy records, we investigated the processes that control fjord sediment inorganic geochemistry through a geochemical, mineralogical and sedimentological analysis of surface sediment samples from the fjords of Northern Chilean Patagonia. A simple Terrestrial Index based on measurements of salinity and Fraction of Terrestrial Carbon was used to estimate the terrestrial input/river discharge at each site. Our results demonstrate that, under the cold climate conditions of Patagonia, chemical weathering is weak and the inorganic geochemical composition of the fjord sediments is primarily controlled by hydrodynamic mineralogical sorting, i.e., the intensity of river discharge. Our results suggest that the distribution of Fe, Ti and Zr in surface sediments is controlled by their association with heavy and/or coarse minerals, whereas Al is independent of hydrodynamic processes. The elemental ratios Fe/Al, Ti/Al and Zr/Al are therefore well suited for estimating changes in the energy of terrestrial sediment supply into the fjords through time. Zr/Al is particularly sensitive in proximal environments, while Fe/Al is most useful in the outer fjords and on the continental margin. In the most proximal environments, however, Fe/Al is inversely related to hydrodynamic conditions. Caution should therefore be exercised when interpreting Fe/Al ratios in terms of past river discharge. The application of these proxies to long sediment cores from Quitalco fjord and Golfo Elefantes validates our interpretations. Our results also emphasize the need to measure Al-based elemental ratios at high precision, which can be achieved using simultaneous acquisition ICP-AES technology. This study therefore constitutes a strong basis for the interpretation of sedimentary records from the Chilean Fjords.

© 2011 Elsevier Ltd. All rights reserved.

## 1. INTRODUCTION

Understanding the causes of past climate variability requires an array of high-resolution paleoclimate records with geographical and chronological resolutions adequate to analyze past patterns of climate dynamics. In this respect, the mid- and high-latitudes of the Southern Hemisphere have been relatively understudied, although

\* Corresponding author at: Renard Centre of Marine Geology, University of Ghent, Krijgslaan 281 s.8, 9000 Gent, Belgium. Tel.: +32 9 264 4637; fax: +32 9 264 4967.

E-mail addresses: [sbertrand@whoi.edu](mailto:sbertrand@whoi.edu), [Sebastien.Bertrand@UGent.be](mailto:Sebastien.Bertrand@UGent.be) (S. Bertrand).

they play a critical role in our understanding of Earth's climate variability. At these latitudes the climate is dominated by the latitudinal position and strength of the Southern Westerly Winds (SWW; Garreaud et al., 2009). Since Southern South America (SSA) is the only continuous land mass in the Southern Hemisphere that intersects the entire westerly wind belt, it constitutes a key region for paleoclimate reconstructions (e.g., Toggweiler, 2009).

Reconstructions of terrestrial climate in SSA are mostly limited to a few lake sedimentary records from Argentina (e.g., Gilli et al., 2005; Mayr et al., 2007), the Chilean Lake District (e.g., Bertrand et al., 2008; Moreno et al., 2010), and the southern tip of Chile (e.g., Moy et al., 2008; Moreno et al., 2010; Waldmann et al., 2010), to discontinuous records of glacial activity (e.g., Kaplan et al., 2008; Moreno et al., 2009) and to a limited number of Late Holocene tree-ring records from Northern Patagonia (e.g., Lara and Villalba, 1993; Villalba et al., 1997). In addition, current paleoceanographic records are limited to a very few sites from the southeastern Pacific, mainly from latitudes around or North of 40°S (e.g., Lamy et al., 2004; Kaiser et al., 2005, 2008; Mohtadi et al., 2007; Muratli, 2010). Very few papers present paleoenvironmental reconstructions based on fjord and near-shore sediments from Chilean Patagonia (Sepúlveda et al., 2009; Lamy et al., 2010; Siani et al., 2010). Our current understanding of past changes in SSA climate remains therefore limited and additional high-resolution and continuous records are critically needed, especially from the “Roaring Forties” latitudes (e.g., Villalba et al., 2009; Moreno et al., 2010).

Motivated by this lack of data, several research teams recently set out to study the sedimentary record of the Chilean Fjords and the adjacent continental margin, and a large number of sediment cores were successfully retrieved during oceanographic cruises, such as the Cimar-7-Fiordo (e.g., Sepúlveda et al., 2009), the NB Palmer 0505 (e.g., Boyd et al., 2008), the R/V Mirai BEAGLE-2003 and MR08-06, and the R/V Marion Dufresne PACHIDERME. Sediments from the Chilean fjords are particularly promising because they present high accumulation rates (Salamanca and Jara, 2003) and can record changes in river discharge (e.g., Sepúlveda et al., 2009), which is linked to precipitation and glacier melting in the Andes (Dávila et al., 2002).

With this in mind, the goal of the current study is to investigate the processes that control sediment geochemistry in the Chilean fjords, with a particular focus on the lithophile and mostly immobile elements Al, Fe, Ti, and Zr (McLennan et al., 2003), since these elements are typically associated to the lithogenic fraction of the sediment and are frequently used as indicators of terrestrial supply in sediment core studies (e.g., Haug et al., 2001; Lamy et al., 2004). After assessing the ability of ICP-AES technology to measure inorganic elemental ratios at high precision, we present geochemical, mineralogical and sedimentological data obtained on a series of surface sediment samples from the fjords of Northern Chilean Patagonia. These multi-proxy analyses, which include the parameters that are the most frequently measured on sediment cores, are then used to discuss (1) the natural parameters that control the bulk composition and the inorganic geochemistry of the

sediment, and (2) the best proxies for reconstructing past changes in the energy of river sediment discharge. We deliberately selected samples from fjords in different geomorphological and glaciological settings since, to be useful for paleoclimate reconstructions, the proposed proxies have to be (1) applicable to sediment cores from any Northern Patagonian fjord, and (2) largely independent of accumulation rates, watershed size, and variations in the nature of the bedrock and soil cover. Our research builds on bulk organic geochemical results previously obtained on surface sediments from the Patagonian fjords (Silva and Prego, 2002; Sepúlveda et al., 2011; Silva et al., 2011), and on multi-proxy studies of surface sediment samples from the Chilean continental margin between 25 and 43°S (Lamy et al., 1998; Hebbeln et al., 2000; Klump et al., 2000; Romero et al., 2001).

## 2. REGIONAL SETTING

The geology of Northern Chilean Patagonia is dominated by the North Patagonian Batholith, which forms the core of the southern Andes and is roughly parallel to the coast (Fig. 1). It is composed of Cenozoic and Mesozoic granitoids, mainly in the form of hornblende-biotite granodiorites and tonalities (Pankhurst et al., 1999; Parada et al., 2007). The batholith is flanked by Mesozoic metamorphic rocks to the West, which form the western side of the Chonos Archipelago and Taitao Peninsula (Fig. 1), and by Mesozoic volcanic rocks to the East (Sernageomin, 2003; Parada et al., 2007). One of the most striking structural features in the region is the Liquiñe-Ofqui fault system, which is responsible for the first-order morphology of the fjords (Glasser and Ghiglione, 2009), and controls the location of the regional volcanoes (Stern et al., 2007). Five of the thirteen Quaternary volcanoes that compose the southern segment of the southern volcanic zone (SSVZ, 42–46°S) are located in our study region (volcanoes Melimoyu, Mentolat, Cay, Macá and Hudson; Fig. 1). Except for Cay volcano, all the SSVZ volcanoes have erupted during the Holocene, Hudson being by far the most active (Stern et al., 2007). These volcanoes are mainly composed of lavas and pyroclasts of basaltic to dacitic composition (Naranjo and Stern, 1998; D'Orazio et al., 2003). The regional soil cover is dominated by andosols, i.e., soils developed on volcanic deposits (Chile, 2003; Gut, 2008). The southern part of the study region is covered by the Northern Patagonian Ice Field (NPI), a 4200 km<sup>2</sup> ice cover that is composed of 70 glaciers larger than 0.5 km<sup>2</sup> (Fig. 1; Rivera et al., 2007).

The morphology of the fjords is complex, with narrow channels and numerous islands separating the mainland from the adjacent Pacific Ocean (Fig. 1). Bathymetric surveys have demonstrated the presence of deep valleys reaching ~600 m at the mouth of the main fjords, and numerous shallow sills of morainic origin (Araya-Vergara, 1997; Rodrigo, 2008). The presence of these sills limits the exchange of bottom waters with the Pacific Ocean, favors high sedimentation rates, and promotes the preservation of organic matter, although anoxic basins have never been observed (Sepúlveda et al., 2005; Silva and Guzman, 2006;

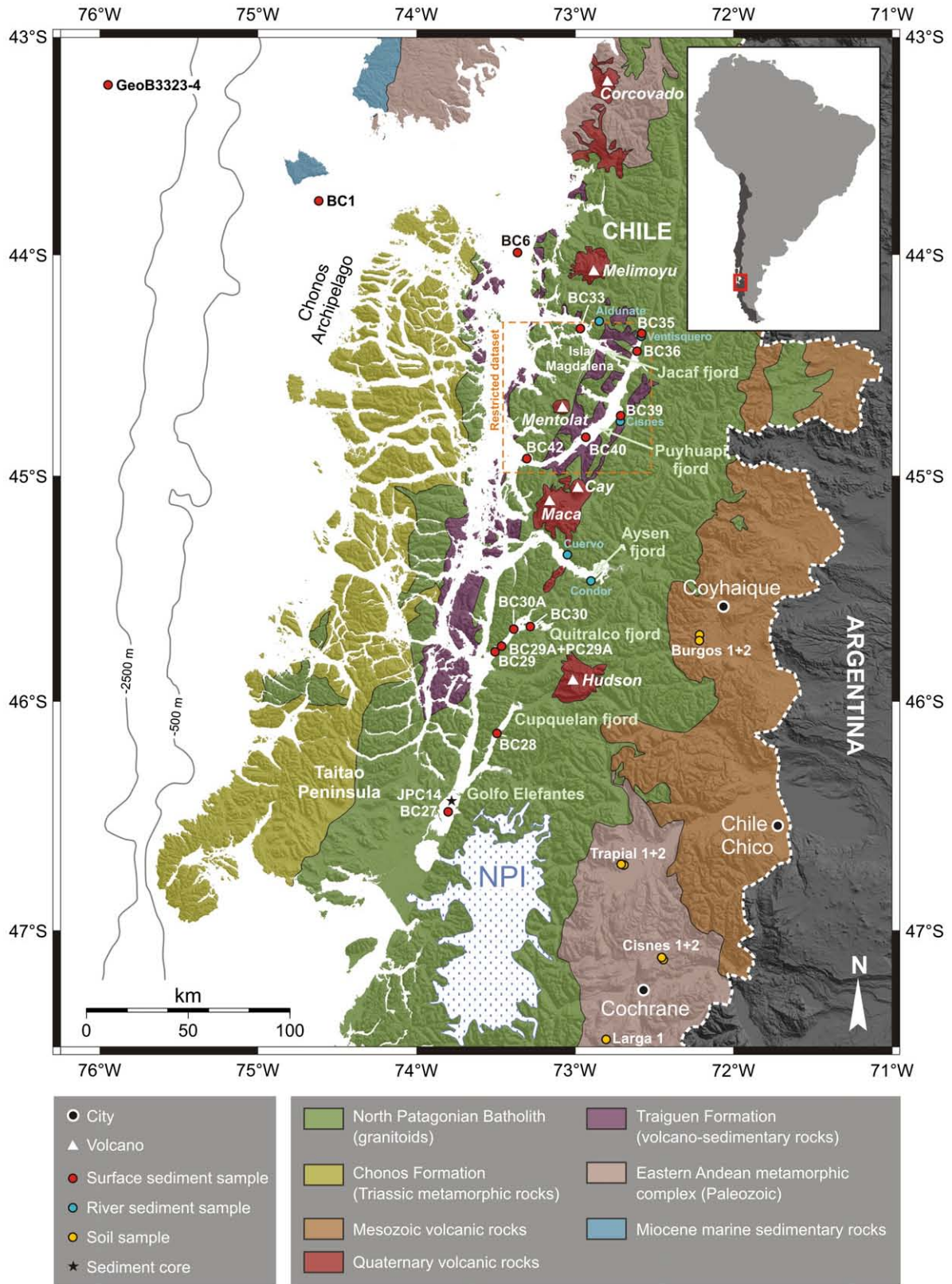


Fig. 1. Location of the sampling sites on a simplified geological map of Northern Chilean Patagonia. The lithological units were drawn according to [Sernageomin \(2003\)](#). Superficial Quaternary deposits were omitted. The bathymetric data are from NDGC-NOAA. The border between Chile and Argentina follows the drainage divide. Sediment core PC29A was collected at the same site than surface sample BC29A. NPI = Northern Patagonian Ice Field.



Sievers and Silva, 2008). Water circulation in the fjords is generally described as a two-layer system, with a surface estuarine water mass (Chilean Fjord Water, CFW) flowing out of the fjords between 0 and ~30 m depth, and a deeper and more saline subantarctic water mass flowing in opposite direction between ~30 and ~150 m depth (Silva and Guzman, 2006; Sievers and Silva, 2008). Where shallow sills do not restrict water circulation, a third deeper and warmer layer composed of modified equatorial subsurface water also occurs (Silva and Guzman, 2006; Sievers and Silva, 2008). The extension and depth of the CFW depends on the amount of freshwater supplied by rivers, glaciers, coastal runoff and direct precipitation, and its salinity reflects the distance from the fresh water sources (Dávila et al., 2002; Sievers and Silva, 2008). The CFW also contributes to the freshening of the northward-flowing Chilean Coastal Current (Strub et al., 1998).

The climate of Northern Chilean Patagonia is strongly oceanic, with high precipitation originating from the combination of the strong SWW with the rough topography of the Andes. Precipitation shows a low seasonality and a strong West-to-East gradient, ranging from ~3000 mm/yr on the western side of the Andes to less than 600 mm/yr at the border with Argentina (Miller, 1976; Aravena and Luckman, 2009). The high precipitation in the area is responsible for a high input of freshwater and terrigenous material to the fjords by river discharge and terrestrial runoff. The fragmentary hydrographic data (Dirección General de Aguas, Chile) show annual average river discharge of 515 and 256 m<sup>3</sup> s<sup>-1</sup> for Rio Aysén and Rio Cisnes, respectively (Calvete and Sobarzo, 2011). Most of the fjords also receive freshwater and terrestrial material from secondary, smaller tributaries located along their profiles. The average air temperature is 8–9 °C, with the highest values occurring in January (13 °C) and the lowest in July (4–6 °C).

### 3. MATERIAL AND METHODS

#### 3.1. Sampling and sample preparation

Surface sediment samples were obtained with a box-corer during the CIMAR (Cruceros de Investigación Marina) 7 Fjords expedition (CF7) in November 2001, aboard the R/V AGOR Vidal Gormaz. Samples were collected at 14 stations between 43.7 and 46.5°S (Fig. 1, Table 1) at depths varying between 52 and 582 m. The sampling stations are roughly located along a terrestrial-marine gradient, from the head of the inner fjords to the break of the continental shelf (Fig. 1). The box-corer samples were sub-sampled on board, using 7-cm diameter PVC tubes, and the samples used in this study consist of a slice of the 0–1 cm depth interval. Samples were stored in plastic bags and frozen at -20 °C until laboratory analyses. Before analysis, all samples were freeze-dried and gently ground and homogenized in an agate mortar. According to <sup>210</sup>Pb profiles, all surface sediment samples represent modern sediments (Rojas, 2002; Salamanca and Jara, 2003; Rebolledo et al., 2005; Sepúlveda et al., 2005; Rebolledo, 2007).

To represent the terrestrial end-member of the sediment, this study uses five river sediment samples that were collected ~100 m upstream of river mouths during the CF7 cruise, and seven samples from four soil profiles that were

collected in the fjord watersheds in 2007 and 2008 (Fig. 1; Table 1). In the laboratory, the river sediment samples were freeze-dried, and the soil samples were oven-dried at 50 °C. These samples were subsequently dry-sieved at 125 µm to discard the coarse particles that are not representative of the sediment fraction that reaches the fjords. They were homogenized in an agate mortar before analysis. Data from the literature (Lamy et al., 1998; Hebbeln et al., 2000; Klump et al., 2000) were used to represent the distal (open ocean) end-member of the sediment.

Finally, samples from sediment cores JPC14 ( $n = 44$ ) and PC29A ( $n = 51$ ), which were collected in Quitralco fjord and Golfo Elefantes, respectively (Fig. 1), were analyzed to test the applicability of our results on long cores. These samples were also freeze-dried and gently ground and homogenized in an agate mortar before geochemical analysis. Sediment core JPC14 (46.449°S–73.798°W) is a 15 m long jumbo piston core that was collected at 129 m depth in the central basin of Golfo Elefantes. The core was taken during cruise NBP05-05 in 2005, on board the RVIB N.B. Palmer. It is composed of a 3 m thick sand unit, surrounded by fine-grained sediment. It covers the last 5400 years and essentially contains sediment delivered by a proglacial river system (Bertrand et al., 2011a). Core PC29A is a 208 cm long piston sediment core collected at station 29A (45.756°S–73.467°W; 112 m depth) during cruise CF7 (see above). It is entirely composed of fine-grained (silt) sediment and it represents the last 1400 years (Bertrand et al., 2011b). It was collected in front of Rio Pelu, a small river that drains a 128 km<sup>2</sup> unglaciated watershed (Ghazoui, 2011).

#### 3.2. Inorganic geochemistry

Samples were prepared using the Li Metaborate fusion technique following Murray et al. (2000), which is preferred over HF digestion because it is the only technique that allows the complete dissolution of sediment samples containing refractory minerals such as zircon (Sholkovitz, 1990; Murray et al., 2000; Huang et al., 2007). Sample preparation consisted in mixing 200 ± 1.0 mg of ultrapure Li-metaborate (SCP Science) in 3 ml Pt:Au (95:5) crucibles, with 50 ± 0.5 mg of sediment. Ten micro liter of 25% LiBr were then added to the mixture and the crucibles were placed in a muffle furnace for 12 min at 1050 °C. The newly formed glass bead was then allowed to cool down for 2–3 min, detached from the crucible, and poured into a Teflon beaker containing a swirling 25 ml solution of 5% HNO<sub>3</sub>. Complete dissolution occurred within ~30 min. The solution was then filtered through a 0.45 µm PVDF Millipore filter and diluted in 5% HNO<sub>3</sub> to obtain a 4000× final dilution. The exact dilution factor was calculated from the precise weight of sediment used for fusion.

Thirteen elements (Electronic Annex EA-1) were measured on a JY Ultima C ICP-AES equipped with a mono- and a poly-chromator that were used in parallel. The analytical conditions (Nebulizer type and flow, pump speed, argon pressure, and gas humidifier) of Murray et al. (2000) were strictly applied. The thirteen elements were analyzed on both the mono- and poly-chromator, except for P, for which no wavelength was available on the polychromator. Measurements were made in triplicates

Table 1  
Location of sampling stations.

Site	Latitude	Longitude	Depth/elevation (m)	Salinity <sup>a</sup> (psu)
<i>Fjord surface sediment samples</i>				
BC1	-43.7517	-74.6215	-240	32.84
BC6	-43.9877	-73.3658	-176	31.18
BC27	-46.4843	-73.8042	-112	22.42
BC28	-46.1408	-73.4955	-239	23.33
BC29	-45.7812	-73.5087	-114	27.67
BC29A	-45.7560	-73.4673	-112	27.59
BC30	-45.6698	-73.2852	-269	27.98
BC30A	-45.6810	-73.3898	-110	27.92
BC33	-44.3335	-72.9695	-582	28.55
BC35	-44.3562	-72.5825	-52	22.24
BC36	-44.4368	-72.6110	-219	23.28
BC39	-44.7273	-72.7145	-160	22.66
BC40	-44.8247	-72.9345	-260	22.40
BC42	-44.9202	-73.3073	-320	28.93
<i>River sediment samples</i>				
Aldunate	-44.3000	-72.8500	0	
Ventisquero	-44.3676	-72.5833	0	
Cisnes	-44.7342	-72.7166	0	
Cuervo	-45.3500	-73.0508	0	
Condor	-45.4666	-72.9008	0	
<i>Soil samples</i>				
Burgos soil 1	-45.7131	-72.2174	+380	
Burgos soil 2	-45.7062	-72.2153	+390	
Trapial soil 1	-46.7126	-72.7110	+265	
Trapial soil 2	-46.7161	-72.6944	+250	
Cisnes soil 1	-47.1166	-72.4550	+435	
Cisnes soil 2	-47.1166	-72.4527	+435	
Larga soil 1	-47.4683	-72.8066	+270	
<i>Open ocean surface sediment sample<sup>b</sup></i>				
GeoB3323-	-43.2183	-75.9500	-3697	

<sup>a</sup> Average of measurements at 2, 5 and 10 m water depth obtained during the second leg of CF7 cruise in November 2001.

<sup>b</sup> From Hebbeln et al. (2000).

and the measured concentrations were corrected for instrumental drift using the measured concentrations of a matrix-matched standard solution ran after every sample. Accuracy and analytical precision (EA-1) were calculated from the analysis of ten individually-prepared sub-samples of reference sediment PACS-2. PACS-2 was selected because its geochemical composition matches the average composition of the fjord sediment samples. The results are presented in Table 2, EA-2 and EA-3.

### 3.3. Bulk organic geochemistry

Approximately 50 mg of ground sediment was weighed in tin capsules and treated with 1 N sulphurous acid to remove eventual carbonates (Verardo et al., 1990). Total Organic Carbon (TOC), Total Nitrogen (TN) and stable isotope ratios of carbon ( $\delta^{13}\text{C}$ ) and nitrogen ( $\delta^{15}\text{N}$ ), were measured at the UC Davis Stable Isotope Facility by continuous flow isotope ratio mass spectrometry (CF-IRMS; 20-20 SERCON mass spectrometer) after sample combustion to  $\text{CO}_2$  and  $\text{N}_2$  at 1000 °C in an on-line elemental analyzer (PDZ Europa ANCA-GSL). The working standards, which are periodically calibrated against international isotope

standards (IAEA N1, N3; IAEA CH7, NBS22), were a mixture of ammonium sulfate and sucrose with  $\delta^{15}\text{N}$  vs Air = 1.33‰ and  $\delta^{13}\text{C}$  vs PDB = -24.44‰. The precision, calculated by replicate analysis of the internal standard, is 0.03‰ for  $\delta^{13}\text{C}$  and 0.08‰ for  $\delta^{15}\text{N}$ . Some of the bulk organic geochemical results used in this study were previously reported in Sepúlveda et al. (2011).

### 3.4. Biogenic opal

Biogenic silica (bio-Si) was analyzed according to Carter and Colman (1994) and Mortlock and Froelich (1989). Samples were extracted with NaOH after removal of organic matter and carbonate with 10%  $\text{H}_2\text{O}_2$  and 1 N HCl, respectively. They were subsequently diluted in 5% nitric acid and analyzed in triplicate for Si, Na and Fe, on a JY Ultima-C ICP-AES. Al was measured in triplicate by flame atomic absorption spectrometry (FAAS) on a Varian SpectraAA 220. Measured Si concentrations were corrected for detrital Si using the measured Al concentrations: bio-Si = measured Si - 2 × Al. The 2:1 ratio accounts for Si leached from volcanic glasses and clay minerals, and this value is similar to the Si:Al ratio measured on soil samples

Table 2  
Geochemical, mineralogical and sedimentological data used in Figs. 2–6.

Sampling station	Depth (m)	TI <sup>a</sup>	Salinity <sup>b</sup> (psu)	F <sub>terr</sub> <sup>c</sup> (wt.%)	Bio-opal (wt.%)	Carbonate (wt.%)	TOC (wt.%)	Lithogenic (wt.%)	Amphibole (wt.%)	Quartz (wt.%)	GS <sup>d</sup> (µm)	MS <sup>e</sup> (10 <sup>-6</sup> SI)	Fe in litho. <sup>f</sup> (wt.%)	Al in litho. <sup>g</sup> (wt.%)	CIA <sup>h</sup>	CIW <sup>i</sup>
<i>Fjord surface sediment samples (n = 14)</i>																
1	240	-2.44	32.84	38.12	3.89	2.14	1.00	91.77	7	16	82.48	6824	4.87	8.61	46.58	48.57
6	176	-1.97	31.18	41.97	7.48	1.89	2.14	85.92	10	21	30.65	2500	5.30	8.59	47.05	46.48
27	112	1.74	22.42	98.85	5.30	0.07	0.51	93.50	14	26	15.40	1407	6.20	8.77	49.64	50.15
28	239	1.22	23.33	88.80	10.02	0.04	0.83	88.11	9	14	7.00	777	6.73	8.96	48.49	45.74
29	114	-1.13	27.67	45.61	8.80	0.06	0.50	90.04	0	6	31.54	1216	5.35	8.95	51.52	45.67
29A	112	-0.27	27.59	70.62	12.36	0.04	1.36	84.61	16	5	21.45	2093	6.02	8.95	47.84	43.89
30	269	-0.12	27.98	77.49	17.56	0.37	3.03	75.41	0	9	17.29	747	6.55	8.00	52.06	40.44
30A	110	-0.55	27.92	64.34	17.69	0.10	2.06	77.68	0	14	12.04	965	6.60	8.52	59.37	41.92
33	582	-0.91	28.55	57.53	11.26	2.04	3.73	78.50	10	15	10.18	710	5.99	8.36	41.39	35.05
35	52	1.28	22.24	84.00	5.86	0.20	2.20	89.09	29	8	19.32	1972	6.99	8.23	40.90	40.63
36	219	1.22	23.28	88.76	4.38	0.32	1.34	92.34	19	20	30.54	2599	6.23	8.62	46.00	45.03
39	160	1.73	22.66	100.00	1.86	0.05	2.74	92.05	6	30	55.45	3061	4.18	8.02	51.48	51.06
40	260	1.51	22.40	91.80	6.92	0.17	2.30	87.83	4	10	43.39	2615	6.01	9.10	47.67	41.77
42	320	-1.31	28.93	47.97	12.18	2.34	2.87	79.15	6	11	18.24	1552	5.59	8.66	43.92	39.65
mean	212	0.00	26.36	71.13	8.97	0.70	1.90	86.14	9	15	28.21	2074	5.90	8.60	48.14	44.00
s.d. <sup>j</sup>	132	1.44	3.57	21.87	4.84	0.93	1.00	6.11	8	7	20.54	1576	0.77	0.35	4.73	4.42
Avg river sed. (n = 5)						0.01	1.69	94.80	30	22	80.78	16,074	7.00	8.56	46.44	48.22
s.d. <sup>j</sup>						0.00	2.26	6.96	12	15	7.48	9403	1.30	0.62	2.49	3.30
Avg soil sed. (n = 7)						0.05	4.18	89.14	0	32	38.73	2214	6.79	10.45	66.73	70.95
s.d. <sup>j</sup>						0.04	1.88	6.33	0	25	8.48	1071	1.44	1.50	6.03	7.24

<sup>a</sup> TI = Terrestrial Index.

<sup>b</sup> Salinity data from leg 2 (spring) of cruise CF7 (November 2001) – data are available on the CENDHOC website ([http://www.shoa.cl/n\\_cendhoc/](http://www.shoa.cl/n_cendhoc/)).

<sup>c</sup> F<sub>terr</sub> = Fraction of Terrestrial Organic Carbon. See Section 4.2 for details.

<sup>d</sup> GS = mean grain size.

<sup>e</sup> MS = magnetic susceptibility.

<sup>f</sup> Fe in litho. = percentage of iron in the lithogenic fraction.

<sup>g</sup> Al in litho. = percentage of aluminum in the lithogenic fraction.

<sup>h</sup> CIA = Chemical Index of Alteration (Nesbitt and Young, 1982), calculated as  $[Al_2O_3 / (Al_2O_3 + CaO + Na_2O + K_2O)] * 100$ , using molecular proportions and after removal of carbonate CaO and salt Na<sub>2</sub>O.

<sup>i</sup> CIW = Chemical Index of Weathering (Harnois, 1988) calculated as  $[Al_2O_3 / (Al_2O_3 + CaO + Na_2O)] * 100$ , using molecular proportions and after removal of carbonate CaO and salt Na<sub>2</sub>O.

<sup>j</sup> s.d. = standard deviation (1 sigma).

prepared with the same technique. This correction assumes that all Al originates from the dissolution of detrital particles. The analytical precision, determined from five entirely separate analyses of a sediment sample from site BC29A, was 1.15% for Si and 3.23% for Al. The precision for bio-Si, i.e. after correction for detrital Si, reached 0.46 wt.%, which indicates that the correction procedure also corrects for uncertainties associated with sample preparation. Biogenic opal (bio-opal,  $\text{SiO}_2 \cdot n\text{H}_2\text{O}$ , wt.%) was obtained by multiplying the bio-Si values by 2.4 (Mortlock and Froelich, 1989). Lithogenic silica (litho-Si, wt.%) was calculated by difference (Total Si [see Section 3.2] – bio-Si).

### 3.5. Carbonate content

The weight percentage of total inorganic carbon (TIC) in bulk sediment samples was determined using an UIC CM5014 coulometer equipped with a CM5130 acidification module. For each sample, 50–60 mg of sediment was precisely weighed in a 4 ml glass vial and treated with 1.5 ml 1 N  $\text{H}_3\text{PO}_4$  to liberate  $\text{CO}_2$ . The percentage of carbonate was calculated from the TIC data using the following equation:  $\text{CaCO}_3$  (wt.%) = TIC (wt.%)  $\times$  8.33, assuming that 100% of the measured  $\text{CO}_2$  is derived from dissolution of calcium carbonate. The analytical precision, determined from seven entirely separate analyses of a sediment sample from site BC29A, was 0.04%  $\text{CaCO}_3$ .

### 3.6. Grain size

Grain size was measured on the terrigenous fraction of the sediment using a Coulter LS200 laser grain size analyzer. The terrigenous fraction was isolated by treating the samples with boiling  $\text{H}_2\text{O}_2$ , HCl and NaOH, to remove organic matter, carbonates and biogenic silica, respectively. Prior to analysis, samples were boiled with 300 mg of sodium pyrophosphate ( $\text{Na}_4\text{P}_2\text{O}_7 \cdot 10\text{H}_2\text{O}$ ) to ensure complete disaggregation of the particles. The grain size distribution of the samples was measured during 90 s and the arithmetic mean was calculated from the 92 size classes.

### 3.7. Bulk and clay mineralogy

Bulk and clay mineralogy was analyzed by X-ray diffraction (XRD) on a Bruker D8-Advance diffractometer with  $\text{CuK}\alpha$  radiation. A first aliquot was separated and mounted as unoriented powder by the back-side method (Brindley and Brown, 1980), and subsequently scanned by XRD between  $2^\circ$  and  $45^\circ 2\theta$ . Peak intensities were used to quantify ( $\pm 5$  wt.%) the mineral proportions, following Cook et al. (1975). Clay minerals were not identified or quantified on the bulk diffractograms. Although halite was detected in all the surface sediment samples, it was not quantified because it derives from interstitial water salts that precipitated during freeze-drying. Clay mineralogy was analyzed on the decarbonated sediment fraction  $< 2 \mu\text{m}$ . Sample preparation consisted in wet-sieving at  $63 \mu\text{m}$ , decarbonation with 0.01 N HCl, and removal of organic matter with  $\text{H}_2\text{O}_2$ . Samples were then rinsed twice with DI water and the  $< 2 \mu\text{m}$  fraction was separated from the aqueous suspension

using the pipette method (1 cm after 50 min, according to Stokes settling law with  $d = 2.65$ ). Oriented mounts were prepared by the “glass-slide method” (Moore and Reynolds, 1989) and subsequently scanned on the diffractometer between  $2^\circ$  and  $30^\circ 2\theta$  after air drying at room temperature, between  $2^\circ$  and  $30^\circ 2\theta$  after solvation with ethylene-glycol for 24 h, and between  $2^\circ$  and  $15^\circ 2\theta$  after oven-heating at  $500^\circ\text{C}$  during 4 h. In addition, slides solvated with ethylene-glycol were scanned at slow speed between  $23$  and  $27^\circ 2\theta$ . Diffractograms were interpreted according to Petschick et al. (1996) and the mineral proportions were quantified (wt.%) in MacDiff v 4.2.5, following the peak area method of Biscaye (1965). Five clay minerals were identified: smectite, illite, chlorite, kaolinite and vermiculite.

### 3.8. Magnetic susceptibility

Magnetic susceptibility (MS) is one of the most frequently measured parameters on sediment cores, owing to the speed and cost effectiveness of the method. Bulk MS is usually used as an indicator of the concentration of allochthonous mineral matter in sediments (e.g., Sandgren and Snowball, 2001). It is a measure of the net contribution of ferromagnetic (magnetite, hematite, etc.) and paramagnetic (olivine, pyroxene, amphibole, etc.) minerals, with the contribution of the latter being more important when ferromagnetic minerals occur in very low concentrations (Houdra and Kahan, 1991; Sandgren and Snowball, 2001). Volume magnetic susceptibility was measured with a Bartington MS2G single-frequency (1.3 kHz) sensor, connected to a Bartington MS3 meter. Sediment samples were gently packed into 1 ml plastic vials and were analyzed in duplicate.

### 3.9. Statistical analyses

Statistical analyses, including Pearson correlation coefficients,  $p$ -values (two-tailed test of significance), Shapiro-Wilk normality tests, Principal Component Analysis (PCA) and Redundancy Analysis (RDA) were conducted with XLSTAT v. 2010.3 (EA-4 and EA-5). The soil and river sediment samples were not included in statistical analyses to prevent any bias by entirely terrestrial samples. Except where indicated, correlations with  $p < 0.05$  were considered significant. The PCA dataset consisted of the 52 variables that are presented in EA-2. Statistical analyses were also conducted on a restricted dataset including samples from Puyhuapi and Jacaf fjords only (i.e., sites 33, 35, 36, 39, 40 and 42; see Fig. 1) to assess the influence of regional variability in lithology on the geochemical results (EA-5). The results of the RDA were essentially similar to those of the PCA.

## 4. RESULTS AND INTERPRETATION

### 4.1. Analytical precision and elemental ratios

The analytical precision obtained on the elemental concentrations with the polychromator is always better than or similar to the precision obtained with the monochromator

(EA-1). The limits of detection (LODs), on the other hand, are generally, but not systematically, better for the monochromator lines (EA-1). For fjord sediment samples, and for sediment and sedimentary rocks in general, the concentrations of the 13 elements of interest are far above ( $>25\times$ ) the LODs of the poly- and mono-chromator lines (EA-1). The only two exceptions are K (very high LOD on the polychromator due to the broad peak associated to the high wavelength of the K line) and Zr (concentration in most sediment samples is only  $10\text{--}20\times$  LOD). Data obtained with the polychromator lines were therefore selected for Al, Ba, Ca, Fe, Mg, Mn, Na, Si, Sr, and Ti. The monochromator lines were used for P (not available on the polychromator), K (very high LOD on the polychromator) and Zr (the monochromator peak was more stable through time). The final analytical precision on the elemental concentrations is therefore lower than 2% (1 sigma) for all elements, except for P (3.60%) and Zr (4.18%). Accuracy for the selected lines was better than 1% for Al, better than 4% for Fe and Ti and could not be calculated for Zr since no reference value exists for PACS-2 (EA-1).

In sedimentary geochemistry, elemental ratios are frequently used to overcome dilution by organic and/or biogenic phases (e.g., Van der Weijden, 2002). The theoretical precision on elemental ratios is calculated using Eq. (1).

$$\text{RSD}_{a/b} = \sqrt{(\text{RSD}_a)^2 + (\text{RSD}_b)^2} \quad (1)$$

where RSD is the relative standard deviation (analytical precision at 1 sigma divided by mean), and a and b are two elements. The precision measured on the elemental ratios obtained with the monochromator is very similar to the theoretical precision. For Ti/Al, for example, the measured precision is 2.25%, whereas the theoretical precision is 2.16%. For the polychromator, however, the measured precision (e.g., 0.68% for Ti/Al) is always much better than the theoretical precision (e.g., 1.22% for Ti/Al), and is also superior to the precision obtained with the monochromator (EA-1). It is also remarkable that, with the polychromator data, the precision of the elemental ratios (Elt/Al) is systematically better than the precision of the corresponding elemental concentrations (EA-1). This increase in precision for elemental ratios is due to the simultaneous acquisition of the elements, which results in the elimination of the signal variability associated with sample preparation and introduction in the plasma, since all spectral lines are affected in similar ways (Schrage, 1999). In consequence, the flickers in signal intensity simply cancel out as elements are detected simultaneously. This demonstrates that ICP-AES is an ideal technique to measure elemental ratios rapidly and at high precision (from 0.1%), provided the instrument is equipped with a polychromator/simultaneous acquisition system.

#### 4.2. Calculation of a terrestrial index

One of the main objectives of this study is to define one or several geochemical proxies for terrestrial input/river

discharge in the Chilean Fjords. In the modern environment, terrestrial input/river discharge clearly affects (1) surface salinities (Dávila et al., 2002) and (2) the proportion of terrestrial organic carbon in surface sediments (Sepúlveda et al., 2011; Silva et al., 2011). These two variables were therefore used to define a Terrestrial Index (TI), which serves as a reference to evaluate relations between inorganic geochemical results and the energy of the terrestrial river supply. TI is calculated as the score of the first axis of a PCA (Fig. 2) that comprises (1) spring salinity data averaged over the upper 10 m (2, 5 and 10 m depth data, collected during leg 2 of CF7 cruise in November 2001), and (2) the fraction of terrestrial organic carbon ( $F_{\text{terr}}$ ), which is calculated from the N/C ratio of the bulk sedimentary organic matter (Perdue and Koprivnjak, 2007; data in Fig. 3 and Table 2). The inclusion of the  $F_{\text{terr}}$  data ensures that TI is representative of year-round sedimentation, and it limits the influence of particular salinity values that may be affected by short-term or seasonal changes in precipitation and river discharge (only spring salinity data were available). To calculate  $F_{\text{terr}}$ , we defined the aquatic end-member as the N/C value of site GeoB3323-4, which was sampled on the continental margin off the coast of Northern Chilean Patagonia (Fig. 1) by Hebbeln et al. (2000) (N/C = 0.130,  $\delta^{13}\text{C} = -19.86$ ) and the terrestrial end-member as the average of five sediment samples (fraction  $< 125\ \mu\text{m}$ ) collected in rivers that discharge into the fjords (N/C = 0.0624,  $\delta^{13}\text{C} = -27.72$ ). The N/C value obtained on the river samples is very similar to the average of the seven soil samples (N/C = 0.0680) but it is preferred because it is known that N/C ratios are affected by transport in rivers and by

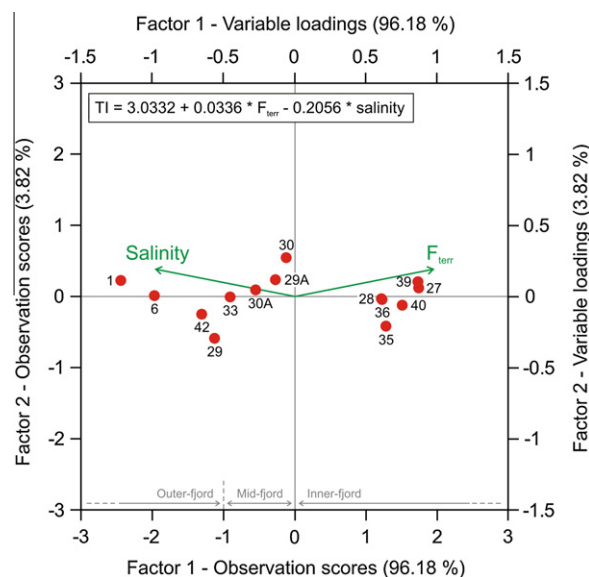


Fig. 2. Results of the principal component analysis (PCA) used to calculate the Terrestrial Index ( $TI = \text{score of PCA axis 1}$ ) from the Fraction of Terrestrial Carbon ( $F_{\text{terr}}$ ) and salinity data. TI can be calculated for any site using the equation indicated on top of the plot, with  $F_{\text{terr}}$  in % and salinity in psu. This equation provides TI values of 6.4 and  $-4.2$  for fully terrestrial (salinity:  $0\text{‰}$ ;  $F_{\text{terr}}$  100%) and fully marine (salinity:  $35\text{‰}$ ;  $F_{\text{terr}}$  0%) environments, respectively.



weathering in soil profiles (Bertrand et al., 2010). Although bulk sedimentary  $\delta^{13}\text{C}$  data can also be used to calculate  $F_{\text{terr}}$  (e.g., Sepúlveda et al., 2011), we prefer using the N/C data because  $\delta^{13}\text{C}$  values of marine organic matter are affected by several processes such as changes in productivity (e.g., Bickert, 2006). The values of  $F_{\text{terr}}$  obtained using the two methods are highly positively correlated ( $r = 0.94$ ,  $p < 0.0001$ ).  $F_{\text{terr}}$  and salinity (2–10 m) are highly correlated ( $r = -0.92$ ,  $p < 0.0001$ , Fig. 3a) and both parameters are independent of sedimentation rates. The resulting TI values, which are linear combinations of  $F_{\text{terr}}$  and salinity, range between  $-2.44$  (BC1) and  $1.74$  (BC27), with positive values indicating a higher terrestrial input (Fig. 2; Table 2). These values were also used to classify the sedimentary environments in inner- ( $\text{TI} > 0$ ), mid- ( $0 < \text{TI} < -1$ ) and outer- ( $\text{TI} < -1$ ) fjords (Fig. 2). The main advantage of this index is that it is sensitive to all types of terrestrial inputs, from direct runoff to small streams and large rivers. This is particularly well illustrated by stations 29 and 29A, which are located only 4.3 km from each other but that have clearly distinct TI values ( $-1.13$ , and  $-0.27$ , respectively) because station 29A is located immediately in front of a small river (Rio Pelu) that discharges into Quitraco fjord.

### 4.3. Sediment composition

#### 4.3.1. Bulk sediment composition

Surface sediments from the fjords of Northern Chilean Patagonia are composed of lithogenic particles ( $86.1 \pm 6.1\%$ ; calculated as  $100\% - \text{bio-opal} - 2.2 \times \text{TOC}$

–  $\text{CaCO}_3$ , e.g., Nederbragt et al., 2008), biogenic opal ( $9.0 \pm 4.8\%$ ), organic matter ( $4.2 \pm 2.2\%$ ; calculated as  $2.2 \times \text{TOC}$ ), and carbonate ( $0.7 \pm 0.9\%$ ) (average  $\pm 1$  s.d.; see Table 2 and EA-2 for data). Distribution plots (Fig. 3b) clearly show that biogenic opal is concentrated in the mid- and outer fjords, while carbonate only occurs in the open ocean and outer fjord sites, where it represents carbonate aquatic productivity. TOC concentrations are very variable and reflect the combined contribution of the terrestrial and aquatic sources of organic matter. In consequence, the lithogenic fraction of the sediment is significantly higher in the inner fjords than further towards the open ocean (Fig. 3b). The absence of carbonate in the river and soil sediment samples provides evidence that all  $\text{CaCO}_3$  originates from aquatic productivity, in agreement with the geological map (Sernageomin, 2003; Fig. 1). Similarly, the low biogenic opal content of the river and soil sediment samples ( $1.47\%$  and  $2.27\%$ , respectively, Fig. 3b and EA-2) compared to the fjord sediment samples ( $9.0 \pm 4.8\%$ ) demonstrates that biogenic opal mainly reflects the fjords productivity in siliceous organisms, predominantly diatoms (Rebolledo et al., 2005). The low amounts of biogenic opal measured in the river and soil sediment samples most likely represent a mixture of siliceous organisms thriving in rivers and fresh volcanic glasses that were not entirely accounted for by the detrital Si correction.

#### 4.3.2. Mineralogy

4.3.2.1. Bulk mineralogy. The bulk mineralogical composition of the surface sediment samples (average  $\pm 1$  s.d.; data in EA-2; Fig. 4a) is dominated by plagioclase ( $42 \pm 10\%$ ,

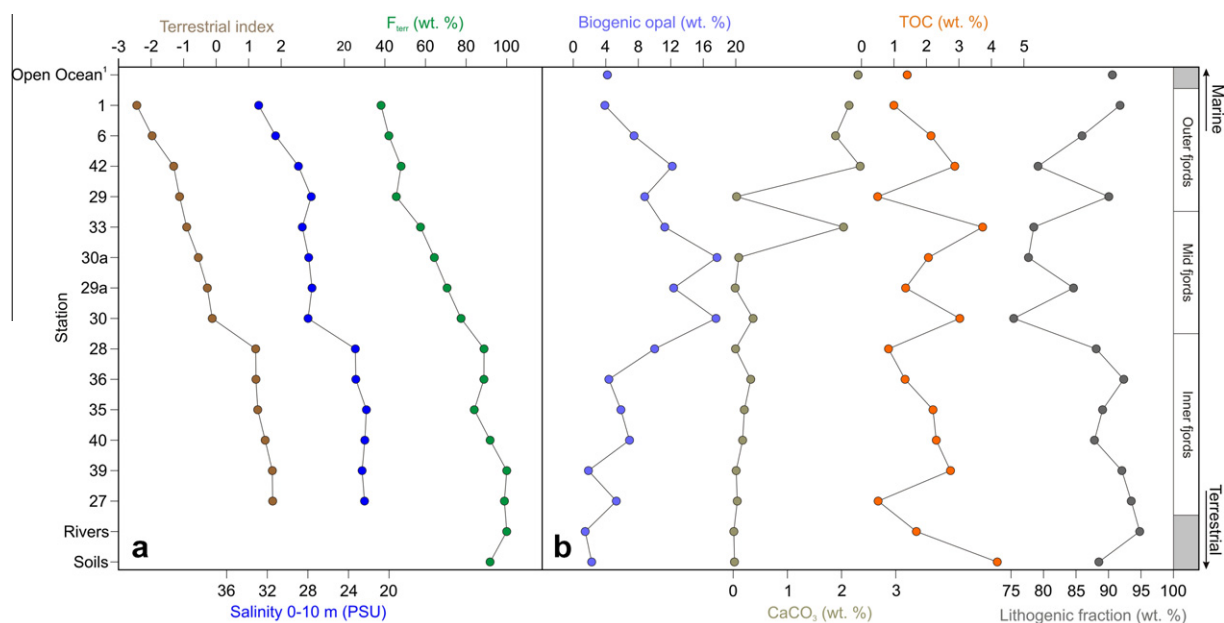


Fig. 3. Spatial variability of indicators of terrestrial input (a), and bulk sediment composition (b). The surface sediment samples are organized according to their Terrestrial Index (TI) in order to visualize the compositional variations along a proximal to distal transect: inner fjord ( $\text{TI} > 0$ ), mid-fjord ( $0 < \text{TI} < -1$ ) and outer fjord ( $\text{TI} < -1$ ). Data are presented in Table 2. See Sections 4.2 and 4.3 for details. (a) Terrestrial Index (TI), salinity (0–10 m), and fraction of terrestrial carbon ( $F_{\text{terr}}$ , %). (b) Bulk sediment composition, expressed as percentages of biogenic opal, Total Organic Carbon (TOC), carbonate and lithogenic fraction. <sup>1</sup>The open ocean data correspond to site GeoB3323-4 off the coast of Southern Chile (Hebbeln et al., 2000; Romero et al., 2001).

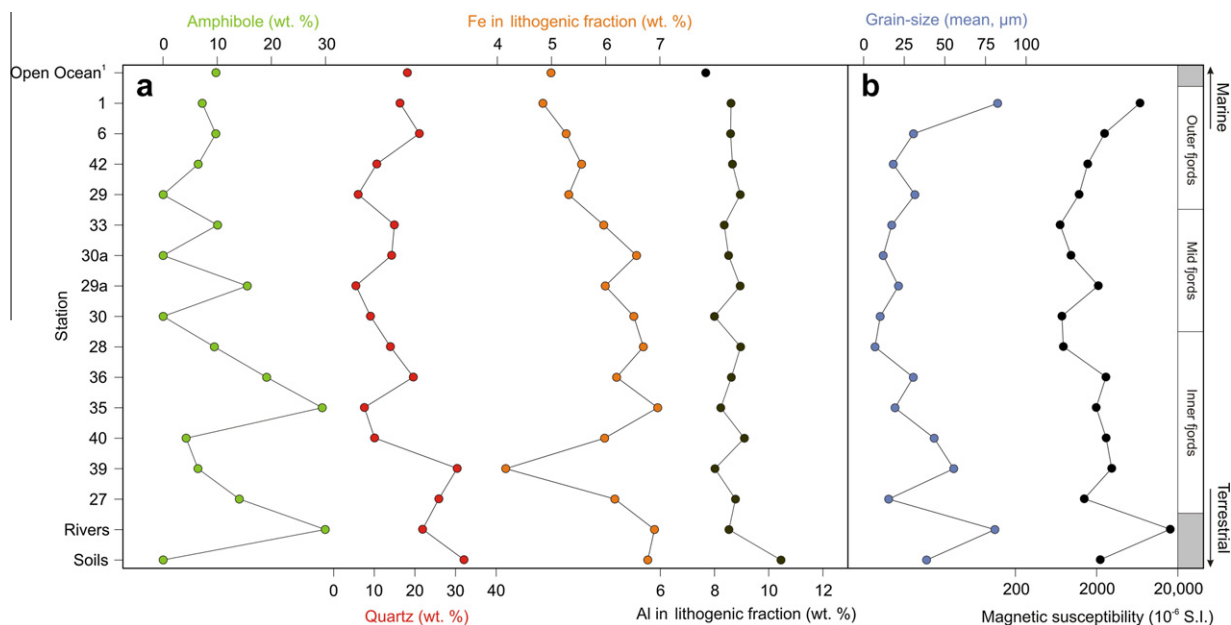


Fig. 4. Spatial variability of selected variables. The samples are organized as in Fig. 3 and the data are presented in Table 2. (a) Selected minerals (amphibole, quartz) and geochemical elements (Fe, Al). (b) Grain size and magnetic susceptibility. The magnetic susceptibility values are primarily controlled by the grain size and the lithogenic content of the sediment. See Section 4.3.5. <sup>1</sup>The open ocean data correspond to site GeoB3323–4 off the coast of Southern Chile (Lamy et al., 1998; Klump et al., 2000). The grain size data of Lamy et al. (1998) were not used since these authors analyzed the silt fraction (2–63  $\mu\text{m}$ ) only.

alkali feldspars ( $20 \pm 7\%$ ), and quartz ( $15 \pm 7\%$ ). Accessory minerals detected by XRD include amphibole ( $9 \pm 8\%$ ), pyroxene ( $10 \pm 6\%$ ), and calcite ( $4 \pm 4\%$ ). Plagioclase was also the dominant mineral in the soil ( $39 \pm 9\%$ ) and river ( $45 \pm 7\%$ ) samples, but alkali feldspar was only detected in 3 soil samples (Burgos 1, Burgos 2, and Trapial 1). Quartz was relatively abundant in the soil ( $32 \pm 25\%$ ) and river ( $22 \pm 15\%$ ) sediment samples, while amphibole was abundant in the river sediment samples ( $30 \pm 12\%$ ) but was below detection limits in the soil samples (Fig. 4a). Calcite was always absent from the river and soil sediment samples and traces of pyroxene were detected in all the soils samples and in some of the river sediment samples (EA-2).

The presence in high proportions of plagioclase, alkali feldspar and pyroxene in the soil samples (EA-2) reflects their volcanic origin (Bertrand and Fagel, 2008), in agreement with the soil map of Gut (2008). In addition, the presence of quartz and the absence of amphibole in these samples most likely reflects the alteration of the underlying bedrock which results in the dissolution of amphibole and in the incorporation of quartz grains in the volcanic ash soils. The high amount of feldspars (plagioclase and alkali feldspar) in the two Burgos soil samples ( $82 \pm 5\%$ ) confirms the dominating volcanic nature of soil parent material in this area, which is frequently affected by explosive eruptions of Hudson, Cay and Maca volcanoes (Chile, 2003; Fig. 1). This interpretation is confirmed by the absence of quartz, and the presence of a broad XRD amorphous diffraction band, which is typical for soils developed on pure volcanic deposits (Bertrand and Fagel, 2008).

For the river and fjord sediment samples, the average proportions of plagioclase, alkali feldspar, pyroxene and

quartz are representative of a mixture of the volcanic (andosol) and granodioritic sources. The presence of significant amounts of amphibole in these samples reflects the importance of the granodioritic source since amphibole is generally absent from regional volcanic ash deposits (Bertrand and Fagel, 2008) but commonly occurs as Hornblende in the rocks of the North Patagonian Batholith (Nelson et al., 1988; Pankhurst et al., 1999). It was however not possible to quantify the contribution of these two main sources based on our mineralogical results since no quantitative mineralogical data exists for the North Patagonian Batholith.

The only minerals that show significant ( $p < 0.05$ ) linear correlations with TI are alkali feldspar ( $r = -0.57$ ), which increases towards the open ocean, and calcite ( $r = -0.65$ ), which only occurs in the open ocean and outer fjord samples, in agreement with the carbonate content data. Amphibole and quartz also decrease towards the open ocean (Fig. 4a), but these relations are not significant at  $p < 0.05$ . An explanation for the concentration of quartz and amphibole in the inner fjords samples is their refractory and density properties (Galy and France-Lanord, 2001; Nesbitt and Young, 1996), i.e., quartz is a relatively refractory mineral that is frequently concentrated in the coarse fraction of the sediment and amphibole is relatively dense and can therefore not be transported on long distances. Therefore, only some small grains of these two minerals can be transported to the Pacific Ocean by the CFW.

**4.3.2.2. Clay mineralogy.** The clay mineralogy of the fjord samples is dominated by illite ( $48 \pm 14\%$ ) and chlorite ( $27 \pm 9\%$ ), with minor amounts of smectite ( $12 \pm 14\%$ ) and kaolinite ( $13 \pm 7\%$ ) (average  $\pm 1$  s.d.; data in EA-2).

These proportions seem to be typical for clay minerals at the mid- to high latitudes of the eastern south Pacific (Fütterer, 2006). The dominance of illite and chlorite is explained by physical erosion of the biotite-rich North Patagonian batholith. The high variability in the smectite content of the fjord sediments (0–36%) most likely originates from regional variations in volcanism, since smectite typically originates from the low temperature alteration of volcanic products (Fütterer, 2006). Illite decreases ( $r = 0.55$ ,  $p = 0.04$ ) and smectite increases ( $r = -0.62$ ,  $p = 0.02$ ) towards the Pacific Ocean. Kaolinite and chlorite do not show any significant trend.

#### 4.3.3. Grain size

The grain size of the lithogenic fraction shows a general decreasing trend towards the open ocean (Fig. 4b; data in Table 2 and EA-2). The only two exceptions are the fine-grained sediments at site 27, which is located in front of a pro-glacial river and therefore mainly receives fine glacial clays and silts, and the sand-dominated sample from site 1, which is located at a depth of 240 m in front of Guafo Island, where strong currents are frequent (Sievers and Silva, 2008), and where steep slopes may result in the development of mass-wasting deposits. The relation between grain size and TI is very well expressed in the restricted dataset ( $r = 0.76$ ,  $p = 0.08$ ).

#### 4.3.4. Inorganic geochemistry

##### 4.3.4.1. Elemental concentrations and selection of an element representative of the lithogenic fraction.

Among the thirteen measured geochemical elements, only Al is positively correlated with the lithogenic fraction of the sediment at  $p < 0.05$  ( $r = 0.90$ ,  $p < 0.001$ ; EA-4). This observation implies that the Al content of the lithogenic fraction of the sediment is almost constant for the entire fjord region (Fig. 4a). It does not vary with TI ( $r = 0.03$ ; Fig. 4) or with grain size ( $r = 0.04$ ). In addition, the Al concentration of the river sediment samples ( $8.09 \pm 0.48\%$ ) varies little and is similar to the Al concentration of the North Patagonian Batholith ( $8.16 \pm 1.16\%$ , data from Pankhurst et al., 1999) and of the Quaternary volcanic rocks ( $8.87 \pm 0.63\%$ , data from Naranjo and Stern, 1998 and D'Orazio et al., 2003). The only source that has higher Al concentrations is the regional volcanic soils ( $9.25 \pm 0.98\%$ ), where Al is concentrated during pedogenesis (preferential dissolution of K, Na, Mg and Ca-rich minerals; Nesbitt and Young, 1989). The similar Al concentrations of the fjord, river and regional rock samples is due to the lithogenic and immobile nature of Al, and its presence in similar concentrations in most igneous and metamorphic rock-forming minerals (Calvert et al., 2001; McLennan et al., 2003). The difference with the soil samples most likely indicates that the contribution of soil material to sedimentation in the fjords is relatively minor. Al is therefore relatively insensitive to changes in the nature of sediment sources, catchment size, and hydrodynamic sorting. As a result, Al is the ideal element to represent the lithogenic fraction of the sediment, and to use as a normalizer for other lithophile elements. Although Fe, Ti and Zr are also generally considered as lithophile and immobile elements (McLennan et al., 2003), they only show weak and

statistically insignificant positive linear correlations with the lithogenic content of the sediment ( $r = 0.22$  to  $0.39$ ).

##### 4.3.4.2. Geochemical ratios, Terrestrial Index and grain size.

In the following we analyze changes in the composition of the lithogenic fraction of the sediment by examining the behavior of Al-based elemental ratios (Elt/Al) and Ti/Fe, Zr/Fe, Zr/Ti. We specifically evaluate the relations between these elemental ratios and TI and grain size (Fig. 5).

None of the elemental ratios are linearly correlated with TI at  $p < 0.05$  (EA-4). The only two weakly significant correlations are with Ca/Al ( $r = -0.51$ ,  $p = 0.06$ ) and Si/Al ( $r = -0.51$ ,  $p = 0.06$ ). However, these two negative correlations do not reflect a change in the lithogenic fraction, but they are due to the global increase in carbonate (Ca/Al) and biogenic silica (Si/Al) productivity towards the outer fjords. Although the composition of the lithogenic fraction is not linearly correlated with TI, elemental ratios Fe/Al, Ti/Al and Zr/Al seem to increase and subsequently decrease towards the marine environment (Fig. 5), with the slope of the decreasing side of the paraboloid being steeper for Zr/Al than for Ti/Al, which is itself steeper than for Fe/Al.

Grain size, on the other hand, is strongly positively correlated with litho-Si/Al ( $r = 0.74$ ,  $p = 0.003$ ; EA-4), which supports the interpretation that quartz is concentrated in the coarse fraction of the sediment (see Section 4.3.2.1). Grain size is also negatively correlated with Fe/Al ( $r = -0.71$ ,  $p = 0.005$ ), which implies that Fe-rich minerals are concentrated in the fine fraction of the sediment. The other elemental ratios do not show significant linear correlations with grain size.

##### 4.3.5. Magnetic susceptibility

In the surface sediment samples, magnetic susceptibility (MS) displays strong variations that are remarkably parallel to the grain size of the lithogenic fraction of the sediment ( $r = 0.93$ ,  $p < 0.0001$ ; Figs. 4b and 6; data in EA-4). A few geochemical elements are significantly correlated with MS, but the most significant correlation is with litho-Si/Al ( $r = 0.67$ ,  $p = 0.009$ ), which confirms that the MS of Chilean fjord sediments is mainly driven by grain size. This high correlation is confirmed by the restricted dataset ( $r = 0.86$ ,  $p = 0.03$  for MS vs litho-Si; EA-5). This restricted data set also displays a highly significant correlation between MS and the lithogenic fraction of the sediment ( $r = 0.89$ ,  $p = 0.02$ ), and between MS and grain size ( $r = 0.91$ ,  $p = 0.01$ ). As a consequence, MS is positively correlated to the combination of grain size and the lithogenic fraction of the sediment ( $r = 0.97$ ,  $p = 0.01$ ; Fig 6b). In the restricted dataset, MS is also highly correlated with TI ( $r = 0.86$ ,  $p = 0.03$ ).

We assume that the relation between MS and the combination of grain size and the lithogenic fraction of the sediment is due to (1) signal dilution by non-lithogenic particles, and (2) enrichment of heavy ferromagnetic minerals in the coarse fraction of the sediment during sedimentary sorting (McLennan et al., 2003). An alternative hypothesis for the significant correlation between MS and grain size is the presence of micro-inclusions of magnetite (Scofield and Roggenthen, 1986) in refractory, and

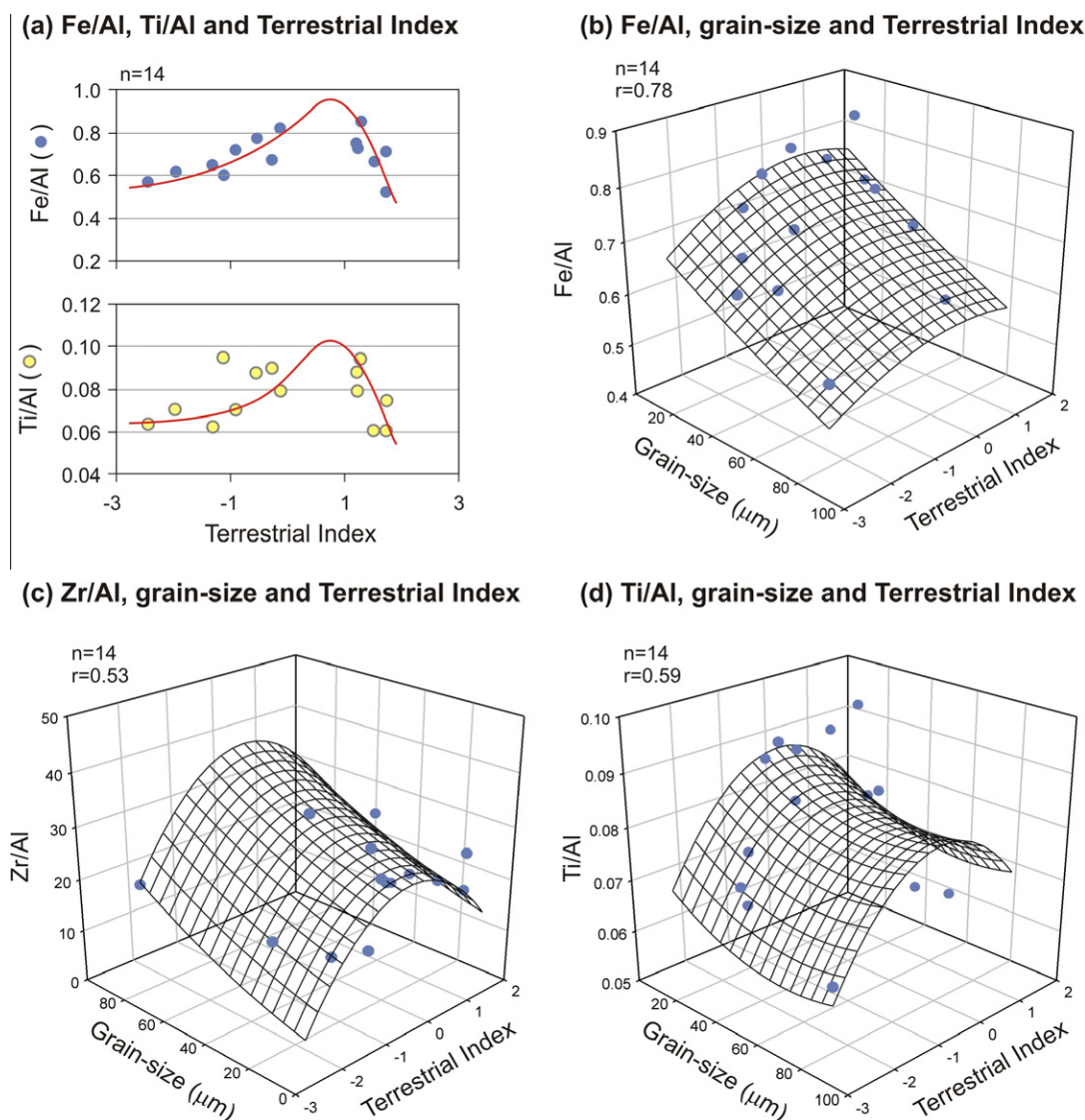


Fig. 5. Relationships between elemental ratios (Fe/Al, Ti/Al and Zr/Al, in g/g) and grain size and the Terrestrial Index for the full dataset. The trends shown in red in (a) do not correspond to any mathematical function and have therefore no statistical value. Note that the grain size scale on the Zr/Al plot is inverted for clarity. The correlation coefficients ( $r$ ) apply to paraboloids fitting through the points. The slope towards negative TI values (distal environment) is steeper for Zr/Al than for Ti/Al, which is in turn steeper than for Fe/Al. (For interpretation of the references to colour in this figure legend, the reader is referred to the web version of this article.)

therefore coarse, minerals usually considered as paramagnetic. Although Andrews (2008) observed a correlation between some paramagnetic minerals and MS in the Denmark Strait, more specific analyses need to be performed to refine this relation.

#### 4.3.6. Principal component analysis

The results of the PCA on the full dataset show a complex structure, with the first two PCA axes accounting for a mere 51.07% of the total variance (Fig. 7a). The first axis primarily reflects variance in (1) Si and Litho-Si, (2) Al and the lithogenic fraction, and, to a lesser extent, (3) Zr, Ti/Fe, Zr/Fe, and Zr/Ti. The loadings of TI and grain size on PCA axis 1 are low, but these two variables load nearly equally on both F1 and F2. Calcite,  $\delta^{15}\text{N}$ ,  $\delta^{13}\text{C}$ , Ca/Al, and

the carbonate content of the sediment load negatively on both F1 and F2, in opposite direction of TI. These variables are associated with salinity and depth, which are indicative of an increased marine influence. Fig. 7a also depicts the combined influence of TI and grain size on a series of variables, such as Ti/Fe, Zr/Fe, Zr/Ti, and pyroxene. The PCA biplot also displays the relatively tight grouping of Litho-Si, Litho-Si/Al, quartz and grain size, which confirms that grain size exerts a strong control on these three geochemical variables. Similarly, a tight grouping is observed for Ti, Zr/Al, and TI. Except for P and P/Al, which are indicators for the presence of the relatively dense mineral apatite, no variable has a strong F2 loading.

On the restricted dataset, the first two PCA axes account for a cumulative 73.22% of the variance, with PCA axis 1



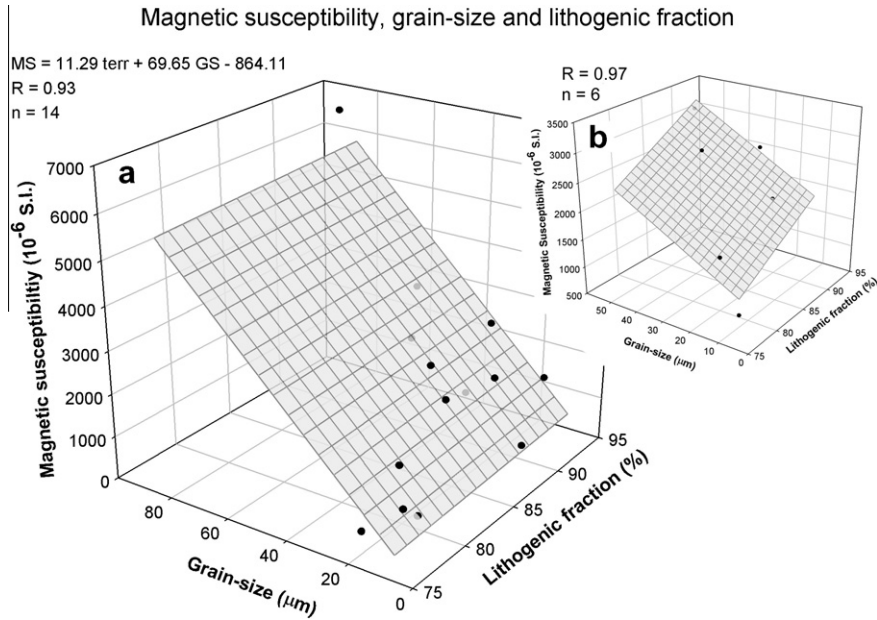


Fig. 6. 3-D correlation plot of magnetic susceptibility vs lithogenic content of the sediment and grain size. (a) Full dataset; (b) Restricted dataset (Jacaf and Puyhuapi fjords).

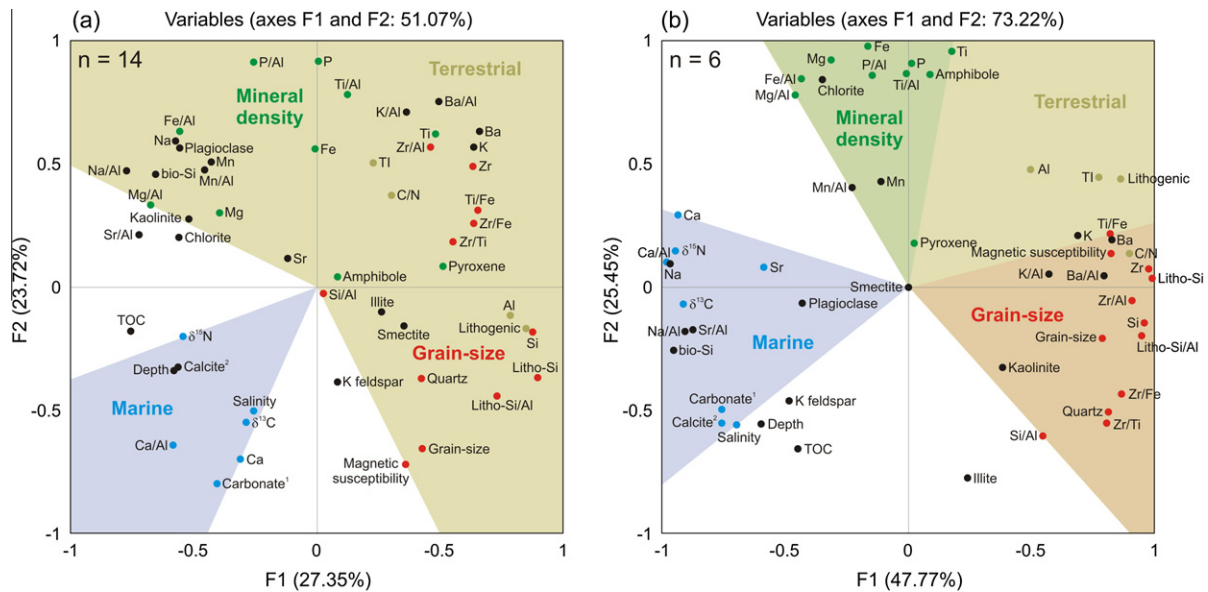


Fig. 7. Principal component analysis (PCA) biplot showing the relationships between the 52 measured variables. (a) Full dataset ( $n = 14$ ); (b) Dataset restricted to samples from Jacaf and Puyhuapi fjords ( $n = 6$ ). The green and red colors highlight the variables that are controlled by mineral density (Fe, Fe/Al, Ti, Ti/Al, Mg, Mg/Al, P, P/Al, amphibole, and pyroxene), and grain size (mean grain size, quartz, Si, Si/Al, Litho-Si, Litho-Si/Al, Zr, Zr/Al, Zr/Ti, Ti/Fe and magnetic susceptibility), respectively. Brown represents more terrestrial and blue more marine sediments. Black dots correspond to variables with no clear affinity. The variables appear better grouped on the plot corresponding to the restricted dataset (b), where specific data clusters can clearly be identified. The plots demonstrate that the variables related to grain size and mineral density are not related but that they are both partly controlled by TI. See Section 4.3.6 for details. <sup>1</sup>Carbonate content measured by coulometry; <sup>2</sup>Calcite wt.% measured by X-ray diffraction. (For interpretation of the references to colour in this figure legend, the reader is referred to the web version of this article.)

explaining nearly half (47.77%) of the total variance. The PCA biplot of the restricted dataset (Fig. 7b) shows a similar pattern to the PCA biplot of the full dataset, but with

much higher F1 loadings for TI and grain size (0.78 and 0.79, respectively). This results in a tighter grouping of the variables controlled by these two parameters, such as

Ti/Fe, but also Litho-Si, Zr, Si, Litho-Si/Al and Zr/Al, with respective F1 loadings of 0.99, 0.98, 0.96, 0.95, and 0.91. The PCA biplot of the restricted dataset (Fig. 7b) also shows that PCA axis 2 captures most of the variance in Ti, Fe, Ti/Al, Mg, and amphibole, which are typical indicators for mafic minerals, and P and P/Al, which represent apatite. These results demonstrate that the grain size of the sediment and its content in mafic, i.e. dense, minerals are independent variables, although both seem to co-vary with TI.

## 5. DISCUSSION

The main factors that control the mineralogy and geochemical composition of siliclastic sediments are (1) the nature of the provenance, (2) the intensity of physical and chemical weathering and (3) the processes that occur during sediment transport (Nesbitt and Young, 1996). Here, we assess the importance of these three factors for the fjords of Northern Chilean Patagonia.

### 5.1. Provenance

Our mineralogical data suggest that the fjord sediments originate from varying mixtures of (1) volcanic particles from the andosols and (2) minerals from the regional bedrock, which is dominated by granitoids and tonalities of the North Patagonian Batholith (Pankhurst et al., 1999; Parada et al., 2007). In addition, secondary lithologies, such as the Quaternary and Mesozoic volcanic rocks and the volcano-sedimentary rocks of the Traiguén Formation (Fig 1) likely play a role in the supply of sediment to some of the fjords. Since these lithologies are not equally represented in all the watersheds, it is reasonable to expect spatial variations in provenance. However, the results obtained on our river sediment samples demonstrate that the particles that are discharged to the fjords have a relatively constant geochemical composition (e.g., Al:  $8.09 \pm 0.48\%$ ; EA-2) that is in agreement with a mixture of the regional volcanic (Al:  $8.87 \pm 0.63\%$ ) and granitoidic (Al:  $8.16 \pm 1.16\%$ ) sources. The low variability in the concentration of other elements in the river sediment samples (e.g., Fe:  $6.57 \pm 0.82\%$ ; Ti:  $0.83 \pm 0.09\%$ ) confirms the relative homogeneity of the sediment particles supplied to the fjords. This relative homogeneity is explained by the effective mixing of the source rocks and soils during river transport, which results in the smoothing of the relatively variable chemical compositions (e.g., Gaillardet et al., 1999). As a result, the nature of the sediment supplied to the fjords of Northern Chilean Patagonia is relatively independent of regional variations in lithology, drainage areas, soil thickness, volcanic influence, etc.

It is worth noting that drainage areas, soil thickness, volcanic activity, and glacier cover most likely varied during the Holocene. Although modern spatial variations of these parameters do not seem to significantly affect provenance, the amplitude of change of these parameters during the Holocene is relatively unknown. The possibility that provenance changed during the Holocene can therefore not be discarded, and it should be taken into account when interpreting data from long fjord sediment cores. Additional

long-distance sources of sediment transported by aeolian processes may also have significantly affected provenance in drier and windier climate conditions.

### 5.2. Weathering

The presence in important proportions of minerals highly susceptible to chemical weathering such as plagioclase, amphibole and pyroxene in the river and fjord sediment samples (EA-2) demonstrates that the sources of sediment to the fjords are mostly fresh. Low chemical weathering is also confirmed by (1) the clay mineralogy, which is dominated by minerals characteristic of physical weathering (illite and chlorite); and by (2) the low values of the Chemical Index of Alteration (CIA; Nesbitt and Young, 1982) and Chemical Index of Weathering (CIW; Harnois, 1988) calculated for the surface (CIA: 48.1; CIW: 44.0; Table 2) and river sediment samples (CIA: 46.4; CIW: 48.2; Table 2, Fig. 8). These values are typical for fresh material ( $\leq 50$ ; fully weathered materials would have values of 100; Price and Velbel, 2003) and are nearly identical to the values calculated for the granitoids of the North Patagonian Batholith (CIA: 48.8; CIW: 54.3; data from Pankhurst et al. (1999)). Low chemical weathering in Northern Patagonia is due to the combined effect of (1) the characteristic cold climate of the region (Nesbitt and Young, 1996); (2) the regional lithology, i.e. granitoids is one of the less reactive lithologies (White and Blum, 1995); and (3) the recent deglaciation of the region, which results in limited time for chemical weathering of the bedrock.

By comparison, the CIA and CIW indices of the soil samples are significantly higher (CIA: 66.7; CIW: 71.0; Table 2, Fig. 8), which demonstrates that chemical weathering depleted the soils in the most soluble elements (Ca, Mg, Na and K), and enriched them in residual elements such as Al. The low values of the CIA and CIW indices for the river and fjord surface sediment samples compared to the soil samples (Fig. 8) is therefore an additional argument that demonstrates that the soils contribute little to provenance, in agreement with the mineralogical and Al concentration data. This statement is also supported by the A–CN–K and A–CNK–FM triangular plots (Nesbitt and Young, 1989) presented in Fig. 8.

The intensity of chemical weathering most likely varied during the Holocene. However the continuously cold climate of Northern Chilean Patagonia since the last deglaciation (e.g., Kaiser et al., 2005) most likely favored physical over chemical weathering, as higher temperature is needed to increase the rate of chemical weathering. More intense physical weathering, and therefore a higher supply of unaltered minerals, during the deglaciation is very likely. The sediment particles that reach the fjords are therefore mainly fresh, and the distribution of soluble elements such as Na, Mg and K in the fjord sediments mainly reflects mineralogical sorting.

### 5.3. Mineralogical sorting during sedimentary transport

Although inorganic geochemical records are frequently interpreted in terms of past changes in terrestrial supply (e.g., Haug et al., 2001; Lamy et al., 2004), there is still an

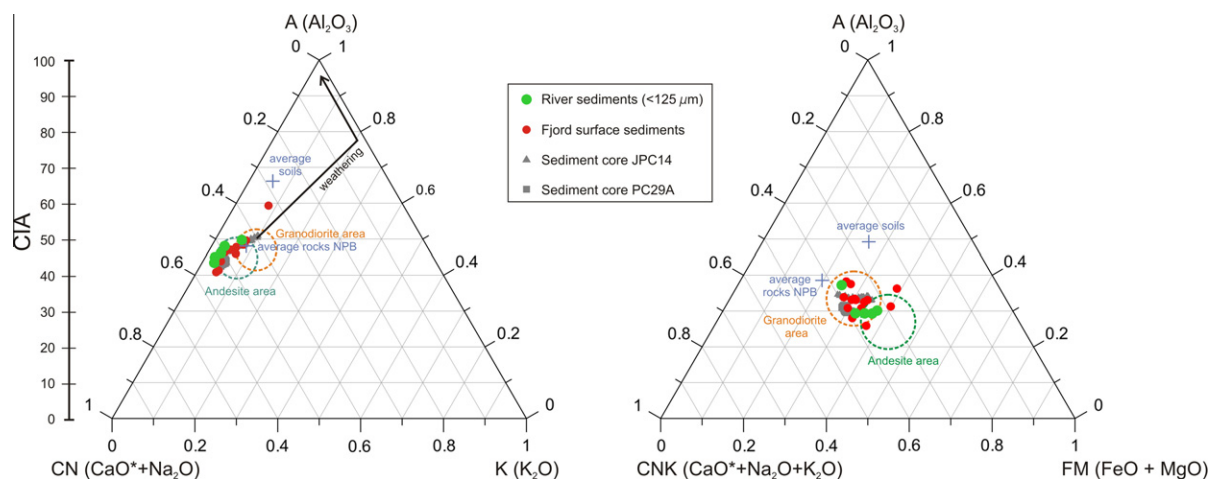


Fig. 8. Ternary plots A–CN–K and A–CNK–FM where A = Al<sub>2</sub>O<sub>3</sub>, C = CaO (silicate fraction only), N = Na<sub>2</sub>O, K = K<sub>2</sub>O, F = total Fe as FeO, and M = MgO (in mole fraction, following Nesbitt and Young (1989)). The weathering trends and the granodiorite and andesite areas are from McLennan et al. (2003). The NPB (North Patagonian Batholith) data are from Pankhurst et al. (1999). CIA = Chemical Index of Alteration (Nesbitt and Young, 1982). The two plots demonstrate that the composition of the river and fjord sediment samples is relatively homogenous, and is similar to the composition of the rocks forming the North Patagonian Batholith. They also demonstrate that the contribution of the regional andosols is minor. Data are presented in Table 2 and EA-2.

evident lack of understanding of the effect of physical processes, mainly sediment transport, on sediment mineralogy and geochemistry. One of the most important studies in this respect is by Nesbitt and Young (1996), who studied the composition of sediments deposited in the fluvio-glacial system of Guys Bight, Baffin Island. These authors found that the primary mafic minerals (olivine, pyroxene, amphibole and biotite) of the bedrock, and therefore Mg and Fe, are enriched in fine sands and muds (i.e., silt + clay), while the coarse sands contain a greater amount of Si. According to Rosenbaum and Reynolds (2004), this distribution probably reflects the small grain size of the heavy mafic minerals of Baffin Island, which makes them hydrodynamically equivalent to less dense minerals such as quartz and feldspar.

Our results from the fjords of Northern Patagonia seem to confirm that grain size and mineral density vary independently, but they also show that both variables are partly related to TI.

In addition, our results show that, among the four lithogenic elements of interest (Al, Fe, Ti, Zr), Al is the only element that clearly reflects the lithogenic content of the sediment. Its distribution is not influenced by grain size or grain density, which means that Al, as a total sum, remains constant in the lithogenic fraction of the fjord sediments. It is therefore independent of sedimentary transport processes. The distribution of Zr, Ti and Fe in the Chilean fjords, however, seems to be controlled by their association with heavy and/or coarse minerals.

Iron is generally associated with relatively dense mafic minerals (amphibole, pyroxene, olivine;  $d = 2.9\text{--}3.5$ ), although it occurs in minor proportions in a large series of minerals, including clays (e.g., Monroe and Wicander, 2009). It is absent from minerals that result from intense weathering, such as kaolinite, which is rare in the Chilean fjords. In environments rich in peat, Fe can also be leached from the peat and transported to sedimentary environments

fixed on Dissolved Organic Carbon (DOC), where it can precipitate as iron-hydroxides (Krachler et al., 2010). In Northern Chilean Patagonia, this source is negligible since peat bogs are much more common south of 48°S (Gut, 2008), and DOC values of North Patagonian streams (0–6 mg/l; Perakis and Hedin, 2002) are one order of magnitude lower than DOC values measured in rivers flowing out of peat bogs (40–70 mg/l; Lal et al., 1997).

Our data show that the distribution of Fe with TI is rather complex (Fig. 5a). The Fe/Al ratio is highest in the inner-fjords with  $0 < TI < 1$ , and it decreases towards the main land ( $TI > 1$ ), as well as towards to open ocean ( $TI < 0$ ). The distribution of amphibole with TI (Fig. 4) being similar to the distribution of Fe/Al with TI, and the close association between amphibole, Mg/Al and Fe/Al in the PCA biplots (Fig. 7) confirm that the distribution of Fe is driven by the concentration of mafic minerals in the mid-fjords. Our results also show that Fe is concentrated in the silt fraction of the sediment (Fig. 5b), in agreement with the observations of Nesbitt and Young (1996) in Guys Bight, and probably due to the low refractoriness of mafic minerals. These data therefore demonstrate that Fe and Mg in the Chilean fjords are associated with sediment particles of low to intermediate grain size and intermediate density. The low concentrations of Fe and Mg in some of the most proximal sites most likely reflect dilution by coarser and/or denser minerals such as quartz. The occurrence of Fe in open marine samples is likely due to its presence in very fine-grained mafic minerals, in plagioclase (density: 2.6–2.7), and in most clay minerals.

Zirconium is most often associated with zircon, which is a typical accessory mineral of the North Patagonian Batholith. Zircon is a very dense ( $d = 4.6\text{--}4.7$ ) and refractory mineral, which results in Zr being concentrated in the densest and coarsest mineralogical fraction of sediments. In Chilean Patagonia, Zirconium concentrations are particularly high in the coarse soil and river sediment samples.

In the fjord sediments, Zr and Zr/Al show a strong association with TI (Fig. 7), which results from its relation with both grain size and density (Fig. 5c). The Zr/Al ratio of sediments is therefore maximum where both grain size and grain density are high, i.e. in the most proximal environments, where the energy of river discharge is maximum. It quickly decreases towards the open ocean (Fig. 5c).

Titanium is frequent in igneous rock-forming minerals (Verhoogen, 1962). It occurs in most mafic minerals (amphibole, pyroxene, olivine;  $d = 2.9\text{--}3.5$ ; Nesbitt, 2003) and in ilmenite, in association with iron, and it is a main constituent of less frequent and relatively dense iron-free minerals such as rutile and titanite (Verhoogen, 1962; Nesbitt and Young, 1996; McLennan et al., 2003;  $d = 3.5\text{--}4.8$ ). Ti is therefore associated with minerals of refractoriness (i.e., grain size) and density similar or higher than Fe-bearing minerals, but lower than Zr-bearing minerals. A direct consequence for sedimentary environments is that the distribution of Ti is similar to that of Fe, although it is transported on smaller distances than the average Fe-bearing minerals. Ti is associated with minerals that are transported on longer distances than zircon (Fig 5d). This is also observed in our dataset, where Ti and Ti/Al are in intermediate position between Fe and Zr (Fig. 5). The behavior of Ti in very proximal (deltaic) environments is not well resolved in our samples but because of its asso-

ciation with mafic minerals, Ti concentrations are expected to decrease in the very coarse and very dense fraction of the sediment. This relation should however be confirmed by studying samples collected in proximal environments at high spatial resolution.

The consequences of these element-mineral associations for the distribution of Al, Fe, Ti and Zr in Chilean fjord sediments are schematically represented in Fig. 9. Proximal locations, such as deltaic environments, contain high amounts of Zr, low amounts of Fe, and intermediate amounts of Ti. The concentrations in Zr quickly decrease towards more distal locations, while the Fe concentrations increase. The inner fjords are characterized by increasing amounts of Ti and Fe. Ti concentrations peak in the mid-fjords and then rapidly decrease towards the open ocean. The highest concentrations in Fe occur at the limit between the mid and outer fjords. In the outer fjords and on the continental margin, the concentrations in Zr and Ti are minimal, and the Fe concentration decreases with distance from the tributaries.

#### 5.4. Proxies of terrestrial sediment discharge

The distribution of the inorganic geochemical elements Al, Fe, Ti, and Zr in the Chilean fjords (Fig. 9) has important implications for inorganic geochemical proxy-records of terrestrial sediment discharge:

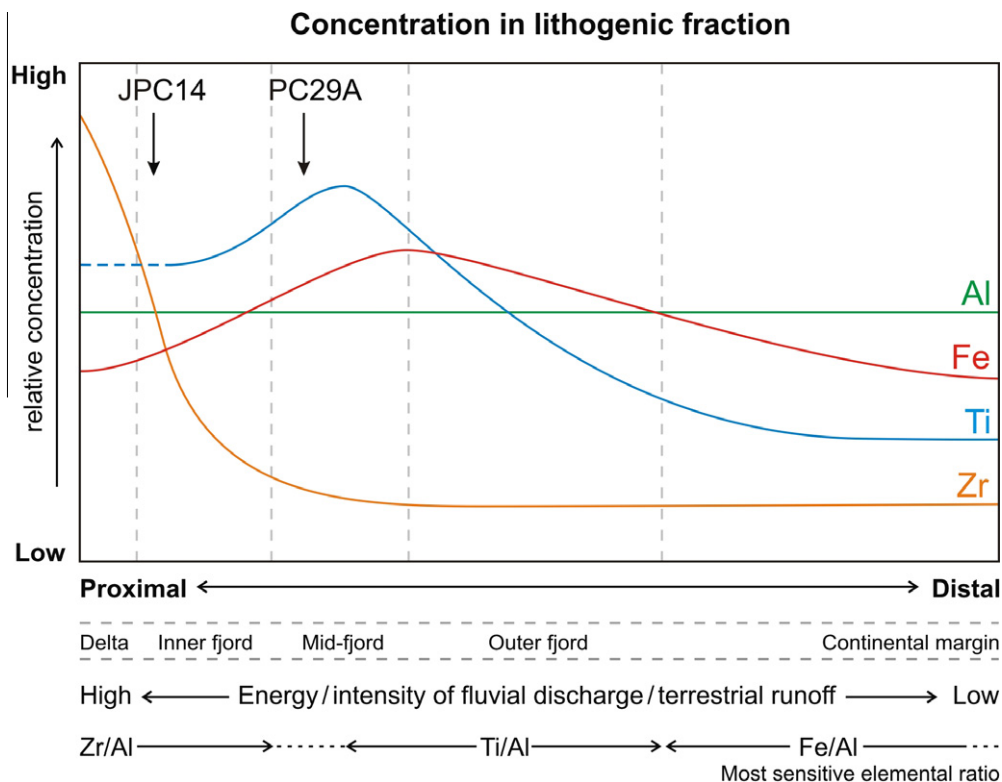


Fig. 9. Schematic representation of the distribution of Al, Fe, Ti and Zr in the lithogenic fraction of the sediment, in relation to distance to the tributaries and energy of the river supply. This illustration demonstrates that not all elemental ratios are sensitive in all types of fjord sedimentary environments. The location of cores JPC14 and PC29A (see Fig. 10) is also indicated. The scale of the vertical and horizontal axes is arbitrary.



- (1) Measuring Al-based elemental ratios at high precision is of utmost importance to accurately calculate variations in the inorganic geochemical composition of terrestrial sediments. For discrete samples, simultaneous acquisition ICP-AES technology is ideal. Although this technique allows the measurement of long sediment cores at reasonable resolution, XRF core scanning is becoming the technique of choice to generate geochemical records at very high resolution. XRF core scanners, however, are limited by their low accuracy for light elements, such as Al (Tjallingii et al., 2007). Technical efforts should therefore be put forward to increase the analytical precision of XRF core scanners for light elements. Substituting Al by Ti or other lithophile elements such as Rb (e.g., Rothwell et al., 2006) may lead to a biased interpretation.
- (2) The elemental ratios Fe/Al, Ti/Al and Zr/Al are well suited for estimating changes in the energy of river discharge into the fjords through time (Fig. 9).
- (3) Not all elemental ratios are sensitive in all environments (Fig. 9). For example, deltaic environments are more sensitive to changes in Zr/Al, than more distal environments, such as outer fjords and continental margins, where Fe/Al is especially useful.
- (4) Caution should be exercised when interpreting Fe/Al data in terms of past river discharge, particularly in proximal environments. The association of Fe with minerals of intermediate grain size and intermediate density results in the non-linearity between Fe/Al and the intensity of river discharge. This relation, which is frequently assumed to be linear when interpreting sediment core records, is only valid for distal locations, where sediments are relatively fine-grained.

The use of elements other than Al, Fe, Ti and Zr to reconstruct past changes in terrestrial supply is less straightforward. Our data demonstrate, for example, that Mg/Al is closely associated to mafic minerals ( $r$  with Fe/Al = 0.91,  $p < 0.001$ ), which indicates that Mg/Al could also be used to reconstruct changes in hydrodynamic conditions in distal environments. However, since Mg is also associated to ocean carbonate productivity (e.g., Raitzsch et al., 2010), this relationship may not be valid where carbonate productivity is high. In addition, our data demonstrate that the litho-Si and quartz contents of the sediment can be used as proxies for grain size. Their use is however restricted to low resolution records since they require either the analysis of discrete samples by XRD, or the measurement of both total Si and bio-Si, which is time-consuming.

In addition to controlling the inorganic geochemical composition of sediments, mineralogical sorting processes also affect other sediment properties, such as magnetic susceptibility. For the Chilean Fjords, our data suggest that MS can be used as a first-order indicator of hydrodynamic changes, since MS is primarily controlled by the grain size of the lithogenic content of the sediment. At sites where the concentration of organic and biogenic particles is high

and potentially variable, MS data should be normalized to the lithogenic fraction (or Al) before being used as a proxy for grain size.

Finally, our data confirm that the bulk organic geochemical composition of the sediment (C/N,  $\delta^{13}\text{C}$ ,  $\delta^{15}\text{N}$ ) remains a powerful tool for assessing terrestrial sediment supply. One of the main advantages of this approach is that it allows the estimation of the relative proportions of marine and terrestrial organic carbon preserved in sediments (e.g., Perdue and Koprivnjak, 2007). Organic-based proxies are however not applicable to sediments with very low TOC, such as those deposited in glacio-marine environments.

### 5.5. Application to sediment cores

To test the validity of our geochemical proxies for paleo-reconstructions, we investigated variations in Fe/Al, Ti/Al and Zr/Al in two long sediment cores collected in two different environments in the fjords of Northern Patagonia. Core JPC14 was collected in front of a pro-glacial river (Fig. 1) and represents an inner-fjord site (TI = 1.74), while core PC29A was collected in the center of Quitalco fjord (TI = -0.27), and is therefore characteristic of a mid-fjord site (Fig. 9). The results (Fig. 10) demonstrate that at site JPC14, Zr/Al is the most sensitive elemental ratio (higher variability, expressed as RSD), while for core PC29A, Ti/Al is the most sensitive. Fig. 10 also clearly demonstrates that at the inner fjord site (JPC14), Zr/Al increases and Fe/Al decreases with increasing hydrodynamic energy, while Ti/Al remains rather insensitive. In core PC29A (mid-fjord site), Zr/Al is rather insensitive, while both Ti/Al and Fe/Al decrease with increasing hydrodynamic energy. These data therefore support our findings that Zr/Al and Ti/Al are the most sensitive elemental ratios in the inner fjords and mid-fjords, respectively. They also confirm that in these proximal environments, Fe/Al is always inversely related to grain size and therefore to hydrodynamic energy.

Furthermore, these results show that the relation between Zr/Al, Ti/Al, Fe/Al and hydrodynamic energy is valid for at least the last 5400 years. Also, the concentrations in the soluble elements Ca, Na and K in the sediment core samples do not change significantly through time, and they suggest that chemical weathering in Northern Patagonia was very limited during the last 5400 years (Fig. 8). Similar low chemical weathering conditions are expected during the deglaciation (17–12 kyr BP; Hulton et al., 2002) since the climate was colder and glaciers were more expanded than during the Neoglaciation (~4500–1000 BP; Glasser et al., 2004). Although temperature was ~2 °C higher during the early Holocene (Heusser and Streeter, 1980; Glasser et al., 2004), this was likely not sufficient to significantly increase chemical weathering rates (Gislason et al., 2009), especially since precipitation decreased concomitantly (Heusser and Streeter, 1980). Given that chemical weathering likely remained low over the deglaciation and Holocene, the proposed proxies of energy of the terrestrial sediment discharge should therefore be valid for the entire period of time recorded by Northern Patagonia fjord sediments.

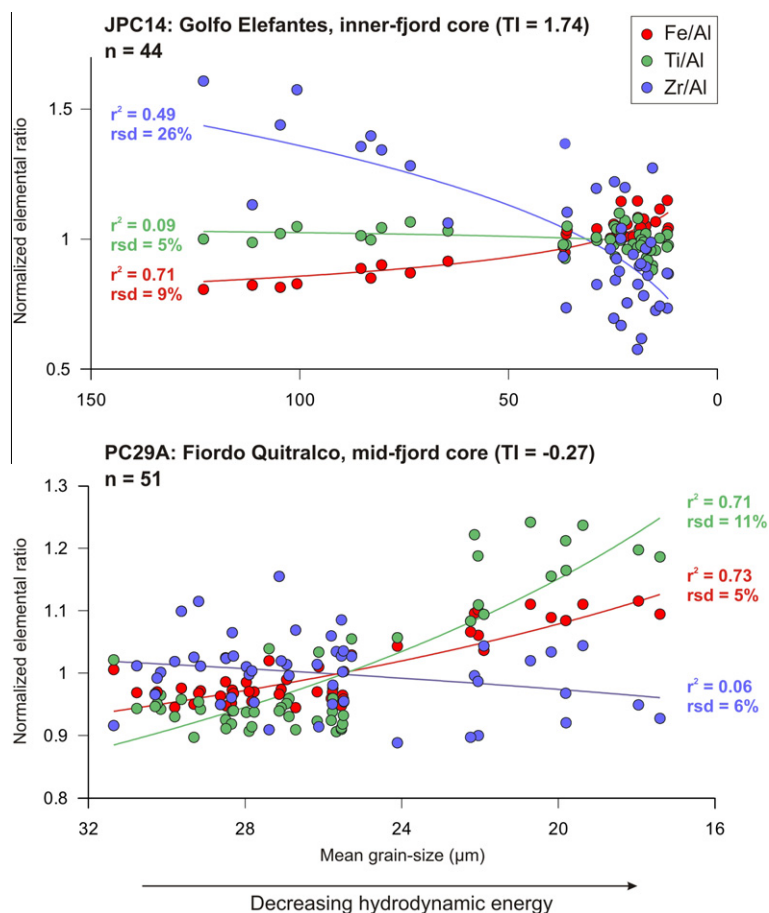


Fig. 10. Normalized elemental ratios (g/g) vs grain size for sediment cores JPC14 (Golfo Elefantes) and PC29A (Quitralco fjord). Grain size is used here as an indicator of hydrodynamic conditions. The relative standard deviation of the normalized data is used to describe the variations between extreme conditions. The determination coefficients ( $r^2$ ) apply to power curves fitting through the points. This figure confirms that Zr/Al and Ti/Al are the most sensitive elemental ratio in the inner fjords and mid-fjords, respectively. Data are presented in EA-3.

## 6. CONCLUSIONS

The inorganic geochemical composition of the sediments deposited in the fjords of Northern Chilean Patagonia is primarily controlled by hydrodynamic mineralogical sorting. Among the four typical lithogenic and mainly immobile elements that are commonly used for the study of past changes in terrestrial input (Al, Fe, Ti, Zr), only Al is independent of hydrodynamic processes. Its concentration reflects the proportion of lithogenic particles, which supports the common practice of normalizing other lithophile elements by Al for assessing changes in the composition of the lithogenic fraction. The distribution of Fe, Ti and Zr is controlled by their association with heavy and/or coarse minerals. Our results show that the sensitivity of Zr/Al, Ti/Al and Fe/Al to changes in the energy of the terrestrial supply to the fjords varies with distance from the tributaries. Zr/Al and Ti/Al are most useful in deltaic and proximal fjord environments, respectively, while increases in Fe/Al can only be translated into higher hydrodynamic conditions in distal environments, such as outer fjords and continental margins. Caution should be exercised when using Fe/Al in proximal environments, where

it shows an inverse relation with the energy of the terrestrial supply. In addition, our data suggest that MS can be used as a first-order indicator of changes in grain size and in the relative proportion of lithogenic particles.

Finally, this dataset constitutes a strong basis for the interpretation of future sedimentary records from the fjords of Chilean Patagonia in terms of past climate and environmental change. The application of the inorganic geochemical proxies developed in this study to long sediment cores should provide important information regarding past changes in river sediment discharge, which is primarily controlled by precipitation and glacier melting. The principles derived from this study may also be applicable to other high-latitude sedimentary basins dominated by inorganic terrestrial inputs.

## ACKNOWLEDGMENTS

We acknowledge the Chilean National Oceanographic Committee (CONA) for financial support to carry out the Cimar-7 Fiordo Program (Grant C7F 01-10 to Silvio Pantoja). The captain and crew of the AGOR Vidal Gormaz are thanked for their professional support during the expedition. The soil samples were collected during a fieldwork expedition led by Dr. Roberto Urrutia

(EULA, Chile), with funding from CONICYT grant 1070508. We thank the curators of the Florida State University Antarctic Marine Geology Research Facility (Simon Nielsen and Lindsey Geary) and John Anderson (Rice University) for providing access to core JPC14. Marco Coolen and Edward Sholkovitz (WHOI) are acknowledged for supplying some of the material used for sample preparation. We are grateful to Maureen Auro, Joanne Goudreau and Olivier Rouxel (WHOI) for their help with the geochemical measurements by FAAS, to Steve Manganini (WHOI) for providing access to the coulometer, to Jan-Berend Stuu and Inka Meyer (MARUM, Bremen, Germany) for sharing the Coulter grain size analyzer, and to Nathalie Fagel (ULg, Belgium) for allowing us to use the x-ray diffractometer. Carina Lange (COPAS, Chile) provided useful comments on an earlier version of this manuscript. This research was supported by a BAEF fellowship (Belgian American Educational Foundation) and an EU FP6 Marie Curie Outgoing Fellowship to S. Bertrand. J. Sepúlveda was supported by Fundación Andes through the WHOI/University of Concepción agreement, and by a scholarship from the Graduate School of the University of Concepción. S. Bertrand is currently a postdoctoral fellow of the Flemish Research Foundation of Belgium. M. Kaplan and one anonymous reviewer are acknowledged for providing constructive reviews.

#### APPENDIX A. SUPPLEMENTARY DATA

Supplementary data associated with this article can be found, in the online version, at doi:10.1016/j.gca.2011.10.028.

#### REFERENCES

- Andrews J. T. (2008) The role of the Iceland Ice Sheet in the North Atlantic during the late Quaternary: a review and evidence from Denmark Strait. *J. Quat. Sci.* **23**(1), 3–20.
- Aravena J.-C. and Luckman B. (2009) Spatio-temporal rainfall patterns in Southern South America. *Int. J. Climatol.* **29**, 2106–2120.
- Araya-Vergara J. F. (1997) Geomorphological profiles of the fjords and longitudinal depression of North Patagonia. *Cienc. Tecnol. Mar.* **20**, 3–22.
- Bertrand S. and Fagel N. (2008) Nature, origin, transport and deposition of andosol parent material in south-central Chile (36–42°S). *Catena* **73**(1), 10–22.
- Bertrand S., Charlet F., Charlier B., Renson V. and Fagel N. (2008) Climate variability of Southern Chile since the Last Glacial Maximum: a continuous sedimentological record from Lago Puyehue (40°S). *J. Paleolimnol.* **39**(2), 179–195.
- Bertrand S., Sterken M., Vargas-Ramirez L., De Batist M., Vyverman W., Lepoint G. and Fagel N. (2010) Bulk organic geochemistry of sediments from Puyehue Lake and its watershed (Chile, 40°S): implications for paleoenvironmental reconstructions. *Palaeogeogr. Palaeoclimatol. Palaeoecol.* **294**, 56–71.
- Bertrand S., Hughen K. A., Lamy F., Stuu J. B. W., Torréjon F. and Lange C. B. (2011a) Precipitation as the main driver of Neoglacial fluctuations of Gualas glacier, Northern Patagonian Icefield. *Clim. Past Discuss.* **7**, 2937–2980.
- Bertrand S., Hughen K. A., Sepúlveda L. and Pantoja S. (2011b) Interactions between precipitation and sea surface temperature in Northern Chilean Patagonia during the Late Holocene. *Mineral. Mag.* **75**, 524.
- Bickert T. (2006) Influence of geochemical processes on stable isotope distribution in marine sediments. In *Marine Geochemistry* (eds. M. D. Schulz and M. Zabel). Springer, Berlin, pp. 339–369.
- Biscaye P. (1965) Mineralogy and sedimentation of recent deep-sea clay in the Atlantic Ocean and adjacent seas and oceans. *Geol. Soc. Am. Bull.* **76**, 803–832.
- Boyd B. L., Anderson J. B., Wellner J. S. and Fernandez R. A. (2008) The sedimentary record of glacial retreat, Marinelli fjord, Patagonia: regional correlations and climate ties. *Mar. Geol.* **255**(3–4), 165–178.
- Brindley G. and Brown G. (1980) *Crystal Structures of Clay Minerals and Their X-ray Identification*. Mineralogical Society of London, UK.
- Calvert S. E., Pedersen T. F. and Karlin R. E. (2001) Geochemical and isotopic evidence for post-glacial palaeoceanographic changes in Saanich Inlet, British Columbia. *Mar. Geol.* **174**, 287–305.
- Calvete C. and Sobarzo M. (2011) Quantification of the surface brackish water layer and frontal zones in southern Chilean fjords between Boca del Guafo (43°30'S) and Estero Elefantes (46°30'S). *Cont. Shelf Res.* **31**(3–4), 162–171.
- Carter S. and Colman S. (1994) Biogenic silica in Lake Baikal sediments: results from 1990–1992 American cores. *J. Great Lakes Res.* **20**(4), 751–760.
- Chile V. (2003) Proyecto Coyhaique XI Región, Chile. Declaración de impacto ambiental. Report for Patagonia Gold Chile S.M.C. p. 117. Available from: <[http://www.e-seia.cl/archivos/digital\\_143483\\_143486\\_1000099.pdf](http://www.e-seia.cl/archivos/digital_143483_143486_1000099.pdf)>.
- Cook H., Johnson P., Matti J. and Zemmels I. (1975) Methods of sample preparation and X-ray diffraction data analysis, X-ray mineralogy laboratory. In *Initial Reports of the DSDP 28* (ed. A. G. Kaneps). DSDP, Washington DC, pp. 997–1007.
- Dávila P., Figueroa D. and Muller E. (2002) Freshwater input into the coastal ocean and its relation with the salinity distribution off austral Chile (35–55°S). *Cont. Shelf Res.* **22**, 521–534.
- D'Orazio M., Innocenti F., Manetti P., Tamponi M., Tonarini S., Gonzales-Ferran O., Lahsen A. and Omarini R. (2003) The quaternary calc-alkaline volcanism of the Patagonian Andes close to the Chile triple junction: geochemistry and petrogenesis of volcanic rocks from the Cay and Maca volcanoes (45°S, Chile). *J. South Am. Earth Sci.* **16**, 219–242.
- Fütterer D. K. (2006) The solid phase of marine sediments. In *Marine Geochemistry* (eds. M. D. Schulz and M. Zabel). Springer, Berlin, pp. 1–25.
- Gaillardet J., Dupré B., Louvat P. and Allègre C. J. (1999) Global silicate weathering and CO<sub>2</sub> consumption rates deduced from the chemistry of large rivers. *Chem. Geol.* **159**, 3–30.
- Galy A. and France-Lanord C. (2001) Higher Erosion rates in the Himalaya: geochemical constraints on riverine fluxes. *Geology* **29**, 23–26.
- Garreaud R. D., Vuille M., Compagnucci R. and Marengo J. (2009) Present-day South American climate. *Palaeogeogr. Palaeoclimatol. Palaeoecol.* **281**(3–4), 180–195.
- Ghazoui Z. (2011). Sédimentation récente dans les fjords de Patagonie Chilienne: caractérisation des sources sédimentaires et implication pour la reconstitution des changements environnementaux au cours de l'Holocène. Unpublished M. Sc. thesis, Department of Geology, Université Libre de Bruxelles, Belgium. 94 pp.
- Gilli A., Ariztegui D., Anselmetti F., McKenzie J. A., Markgraf V., Hajdas I. and McCulloch R. (2005) Mid-Holocene strengthening of the southern westerlies in South America—Sedimentological evidences from Lago Cardiel, Argentina (49°S). *Global Planet. Change* **49**, 75–93.
- Gislason S. R., Oelkers E. H., Eiriksdottir E. S., Kardjilov M. I., Gisladdottir G., Sigfusson B., Snorrason A., Elefsen S., Hardardottir J., Torssander P. and Oskarsson N. (2009) Direct evidence of the feedback between climate and weathering. *Earth Planet. Sci. Lett.* **277**, 213–222.

- Glasser N. F., Harrison S., Winchester V. and Aniya M. (2004) Late Pleistocene and Holocene paleoclimate and glacier fluctuations in Patagonia. *Glob. Planet. Change* **43**, 79–101.
- Glasser N. and Ghiglione M. (2009) Structural, tectonic and glaciological controls on the evolution of fjord landscapes. *Geomorphology* **105**, 291–302.
- Gut B. (2008) *Trees in Patagonia*. Springer, Basel, 283 p.
- Harnois L. (1988) The CIW index: a new chemical index of weathering. *Sed. Geol.* **55**, 319–322.
- Haug G. H., Hughen K. A., Sigman D. M., Peterson L. C. and Röhl U. (2001) Southward migration of the intertropical convergence zone through the Holocene. *Science* **293**, 1304–1308.
- Hebbeln D., Marchant M., Freudenthal T. and Wefer G. (2000) Surface sediment distribution along the Chilean continental slope related to upwelling and productivity. *Mar. Geol.* **164**(3–4), 119–137.
- Heusser C. J. and Streeter S. S. (1980) A temperature and precipitation record of the past 16,000 years in southern Chile. *Nature* **210**, 1345–1347.
- Houdra F. and Kahan S. (1991) The magnetic fabric relationship between sedimentary and basement nappes in the High Tatra Mountains N. Slovakia. *J. Struct. Geol.* **13**(4), 431–442.
- Huang S., Sholkovitz E. and Conte M. (2007) Application of high-temperature fusion for analysis of major and trace elements in marine sediment trap samples. *Limnol. Oceanogr. Methods* **5**, 13–22.
- Hulton N. R. J., Purves R. S., McCulloch R. D., Sugden D. E. and Bentley M. J. (2002) The last glacial maximum and deglaciation in Southern South America. *Quatern. Sci. Rev.* **21**, 233–241.
- Kaiser J., Lamy F. and Hebbeln D. (2005) A 70-kyr sea surface temperature record off southern Chile (ODP Site 1233). *Paleoceanography* **20**. doi:10.1029/2005PA001146.
- Kaiser J., Schefuß E., Lamy F., Mohtadi M. and Hebbeln D. (2008) Glacial to Holocene changes in sea surface temperature and coastal vegetation in north central Chile: high versus low latitude forcing. *Quatern. Sci. Rev.* **27**, 2064–2075.
- Kaplan M. R., Fogwill C. J., Sugden D. E., Hulton N., Kubik P. W. and Freeman S. P. H. T. (2008) Southern Patagonian glacial chronology for the last glacial period and implications for Southern Ocean climate. *Quatern. Sci. Rev.* **27**, 284–294.
- Klump J., Hebbeln D. and Wefer G. (2000) The impact of sediment provenance on barium-based productivity estimates. *Mar. Geol.* **169**, 259–271.
- Krachler R., Krachler R. F., von der Kammer F., Süphandag A., Jirsa F., Ayromlou S., Hofmann T. and Keppler B. K. (2010) Relevance of peat-draining rivers for the riverine input of dissolved iron into the ocean. *Sci. Total Environ.* **408**(11), 2402–2408.
- Lal R., Kimble J. M., Follett R. F. and Stewart B. A. (1997) *Soil Processes and The Carbon Cycle*. CRC Press, Boca Raton (Florida), 624 p.
- Lamy F., Hebbeln D. and Wefer G. (1998) Terrigenous sediment supply along the Chilean continental margin: modern regional patterns of texture and composition. *Geol. Rundsch.* **87**, 477–494.
- Lamy F., Kaiser J., Ninnemann U., Hebbeln D., Arz H. and Stoner J. (2004) Antarctic timing of surface water changes off Chile and Patagonian Ice Sheet response. *Science* **304**, 1959–1962.
- Lamy F., Kilian R., Arz H., Francois J.-P., Kaiser J., Prange M. and Steinke T. (2010) Holocene changes in the position and intensity of the southern westerly wind belt. *Nat. Geol.* **3**(10), 695–699.
- Lara A. and Villalba R. (1993) A 3620-year temperature record from Fitzroya cupressoides tree rings in Southern South America. *Science* **260**, 1104–1106.
- Mayr C., Wille M., Habertzettl T., Fey M., Janssen S., Lücke A., Ohlendorf C., Oliva G., Schäbitz F., Schleser G. H. and Zolitschka B. (2007) Holocene variability of the Southern Hemisphere westerlies in Argentinean Patagonia (52°S). *Quatern. Sci. Rev.* **26**, 579–584.
- McLennan S. M., Bock B., Hemming S. R., Hurowitz J. A., Lev S. M. and McDaniel D. K. (2003) The roles of provenance and sedimentary processes in the geochemistry of sedimentary rocks. In *Geochemistry of Sediments and Sedimentary Rocks: Evolution Considerations to Mineral Deposit-Forming Environments* (ed. D. R. Lentz). Geological Association of Canada, GeoText 4, St. John's, Newfoundland, pp. 7–38.
- Miller A. (1976) The climate of Chile. In *World Survey of Climatology* (ed. W. Schwerdtfeger). Elsevier, Amsterdam, pp. 107–134.
- Mohtadi M., Romero O. E., Kaiser J. and Hebbeln D. (2007) Cooling of the southern high latitudes during the Medieval Period and its effect on ENSO. *Quatern. Sci. Rev.* **26**, 1055–1066.
- Monroe J. S. and Wicander R. (2009) *The Changing Earth: Exploring Geology and Evolution*. Brooks/Cole, Belmont, CA, USA.
- Moore D. and Reynolds R. (1989) *X-ray diffraction and the identification and analysis of clay minerals*. Oxford University Press, Oxford.
- Moreno P. I., Kaplan M. R., Francois J. P., Villa-Martinez R., Moy C. M., Stern C. R. and Kubik P. W. (2009) Renewed glacial activity during the Antarctic cold reversal and persistence of cold conditions until 11.5 ka in southwestern Patagonia. *Geology* **37**, 375–378.
- Moreno P. I., François J. P., Moy C. M. and Villa-Martínez R. (2010) Covariability of the Southern Westerlies and atmospheric CO<sub>2</sub> during the Holocene. *Geology* **38**, 727–730.
- Mortlock R. A. and Froelich P. N. (1989) A simple method for the rapid determination of biogenic opal in pelagic marine sediments. *Deep Sea Res. Part A* **36**, 1415–1426.
- Moy C. M., Dunbar R. B., Moreno P. I., Francois J.-P., Villa-Martinez R., Mucciarone D. M., Guilderson T. P. and Garreaud R. D. (2008) Isotopic evidence for hydrologic change related to the westerlies in SW Patagonia, Chile, during the last millennium. *Quatern. Sci. Rev.* **27**, 1335–1349.
- Muratli J. M., Chase Z., McManus J. and Mix A. (2010) Ice-sheet control of continental erosion in central and southern Chile (36–41°S) over the last 30,000 years. *Quatern. Sci. Rev.* **29**(23–24), 3230–3239.
- Murray R., Miller D. and Kryc K. (2000) Analysis of major and trace elements in rocks, sediments, and interstitial waters by inductively coupled plasma–atomic emission spectrometry (ICP-AES). ODP Technical Note 29.
- Naranjo J. A. and Stern C. R. (1998) Holocene explosive eruption of Hudson Volcano, southern Andes. *Bull. Volc.* **59**, 291–306.
- Nederbragt A. J., Thurow J. W. and Bown P. R. (2008) Paleoproductivity, ventilation, and organic carbon burial in the Santa Barbara Basin (ODP Site 893, off California) since the last glacial. *Paleoceanography* **23**, PA1211. doi:10.1029/2007PA001501.
- Nelson E., Bruce E., Elthon D., Kammer D. and Weaver S. (1988) Regional lithologic variation in the Patagonian batholith. *J. South Am. Earth Sci.* **1**(3), 239–247.
- Nesbitt H. W. (2003) Petrogenesis of siliciclastic sediments and sedimentary rocks. In *Geochemistry of Sediments and Sedimentary Rocks: Evolution Considerations to Mineral Deposit-Forming Environments* (ed. D. R. Lentz). Geological Association of Canada, GeoText 4, St. John's, Newfoundland, pp. 39–51.
- Nesbitt H. W. and Young G. M. (1982) Early Proterozoic climates and plate motions inferred from major element chemistry of lutites. *Nature* **299**, 715–717.



- Nesbitt H. W. and Young G. M. (1989) Formation and diagnosis of weathering profiles. *J. Geol.* **97**, 129–147.
- Nesbitt H. W. and Young G. M. (1996) Petrogenesis of sediments in the absence of chemical weathering: effects of abrasion and sorting on bulk composition and mineralogy. *Sedimentology* **43**, 341–358.
- Parada M., López-Escobar L., Oliveros V., Fuentes F., Morata D., Calderón M., Aguirre L., Féraud G., Espinoza F., Moreno H., Figueroa O., Muñoz Bravo J., Troncoso Vásquez R. and Stern, C. (2007) Andean magmatism. In *The Geology of Chile* (eds T. Moreno and W. Gibbons). Geological Society of London, Bath, pp. 115–146.
- Pankhurst R., Weaver S., Hervé F. and Larrondo P. (1999) Mesozoic-Cenozoic evolution of the North Patagonian Batholith in Aysén, southern Chile. *J. Geol. Soc.* **156**, 673–694.
- Perakis S. S. and Hedin L. O. (2002) Nitrogen loss from unpolluted South American forests mainly via dissolved organic compounds. *Nature* **415**, 416–419.
- Perdue E. M. and Koprivnjak J.-F. (2007) Using the C/N ratio to estimate terrigenous inputs of organic matter to aquatic environments. *Estuar. Coast. Shelf Sci.* **73**(1–2), 65–72.
- Petschick R., Kuhn G. and Gingele F. (1996) Clay mineral distribution in surface sediments of the South Atlantic: sources, transport, and relation to oceanography. *Mar. Geol.* **130**(3–4), 203–229.
- Price J. and Velbel M. (2003) Chemical weathering indices applied to weathering profiles developed on heterogeneous felsic metamorphic parent rocks. *Chem. Geol.* **202**(3–4), 397–416.
- Raitzsch M., Duenas-Bohórquez A., Reichart G.-J., de Nooijer L. J. and Bickert T. (2010) Incorporation of Mg and Sr in calcite of cultured benthic foraminifera: impact of calcium concentration and associated calcite saturation state. *Biogeosciences* **7**, 869–881. doi:10.5194/bg-7-869-2010.
- Rebolledo L. (2007) Variabilidad temporal en la paleoproduktividad durante los últimos ~1800 años en los fiordos chilenos de Patagonia norte (44–46°S). Unpublished Ph. D. Thesis, Department of Oceanography, University of Concepción, Chile. 162 pp.
- Rebolledo L., Lange C. B., Figueroa D., Pantoja S., Muñoz P. and Castro R. (2005) 20th century fluctuations in the abundance of siliceous microorganisms preserved in the sediments of the Puyuhuapi Channel (44°S), Chile. *Rev. Chil. Hist. Nat.* **78**(3), 469–488.
- Rivera A., Benham T., Casassa G., Bamber J. and Dowdeswell J. (2007) Ice elevation and areal changes of glaciers from the Northern Patagonia icefield, Chile. *Global Planet. Change* **59**(1–4), 126–137.
- Rodrigo C. (2008) Submarine topography in the Chilean North Patagonian channels. In *Progress in the oceanographic knowledge of Chilean interior waters, from Puerto Montt to Cape Horn* (eds N. Silva and S. Palma). Comité Oceanográfico Nacional – Pontificia Universidad Católica de Valparaíso, Valparaíso, Chile, pp. 19–23.
- Rojas N. (2002) Distribución de material orgánica, carbono, nitrógeno, y diagénesis temprana en sedimentos de la zona de canales australes entre los golfos Corcovado y Elefantes, Chile. Unpublished M. Sc. thesis, Universidad Católica de Valparaíso, 67 pp.
- Romero O. E., Hebbeln D. and Wefer G. (2001) Temporal and spatial variability in export production in the SE Pacific Ocean: evidence from siliceous plankton fluxes and surface sediment assemblages. *Deep Sea Res. Part I* **48**, 2673–2697.
- Rosenbaum J. G. and Reynolds R. L. (2004) Record of Late Pleistocene glaciation and deglaciation in the southern Cascade Range: II. Flux of glacial flour in a sediment core from Upper Klamath Lake, Oregon. *J. Paleolimnol.* **31**, 235–252.
- Rothwell R. G., Hoogakker B., Thomson J., Croudace I. W. and Frenz M. (2006) Turbidite emplacement on the southern Balearic Abyssal Plain (western Mediterranean Sea) during Marine Isotope Stage 1–3: an application of ITRAX XRF scanning of sediment cores to lithostratigraphical analysis. In *New Techniques in Sediment Cores Analysis* (ed. R. G. Rothwell). Geological Society of London Special Publications, London., pp. 79–98.
- Salamanca M. A. and Jara B. (2003) Distribución y acumulación de plomo (Pb y <sup>210</sup>Pb) en sedimentos de los fiordos de la XI región de Chile. *Ciencia y Tecnología del Mar* **26**, 61–71.
- Sandgren P. and Snowball I. (2001) Application of mineral magnetic techniques to paleolimnology. In *Tracking environmental change using lake sediments, volume 2: Physical and chemical methods* (eds W. Last and J. Smol). Kluwer Academic Publishers, Dordrecht, pp. 217–237.
- Schrag D. P. (1999) Rapid analysis of high-precision Sr/Ca ratios in corals and other marine carbonates. *Paleoceanography* **14**(2), 97–102.
- Scofield N. and Roggenthen W. M. (1986) Petrologic evolution of plagioclase-rich cumulates from the Wichita Mountains, Oklahoma: effects upon magnetic remanence properties. *Geology* **14**, 908–911.
- Sepúlveda J., Pantoja S., Hughen K., Lange C., Gonzalez F., Muñoz P., Rebolledo L., Castro R., Contreras S., Ávila A., Rossel P., Lorca G., Salamanca M. and Silva N. (2005) Fluctuations in export productivity over the last century from sediments of a southern Chilean fjord (44°S). *Estuar. Coast. Shelf Sci.* **65**, 587–600.
- Sepúlveda J., Pantoja S., Hughen K. A., Bertrand S., Figueroa D., León T., Drenzek N. J. and Lange C. (2009) Late Holocene sea-surface temperature and precipitation variability in northern Patagonia, Chile (Jacaf Fjord, 44°S). *Quatern. Res.* **72**, 400–409.
- Sepúlveda J., Pantoja S. and Hughen K. A. (2011) Sources and distribution of organic matter in northern Patagonia fjords, Chile (44–47°S): a multi-tracer approach for carbon cycling assessment. *Cont. Shelf Res* **31**(3–4), 315–329.
- Sernageomin (2003) Mapa geológico de Chile version digital, escala 1/1.000.000.
- Sholkovitz E. (1990) Rare-earth elements in marine sediments and geochemical standards. *Chem. Geol.* **88**(3–4), 333–347.
- Siani G., Colin C., Michel E., Carel M., Richter T., Kissel C. and Dewilde F. (2010) Late Glacial to Holocene terrigenous sediment record in the Northern Patagonian margin: paleoclimate implications. *Palaeogeogr. Palaeoclimatol. Palaeoecol.* **297**(1), 26–36.
- Sievers H. and Silva N. (2008) Water masses and circulation in austral Chilean channels and fjords. In *Progress in the oceanographic knowledge of Chilean interior waters, from Puerto Montt to Cape Horn* (eds N. Silva and S. Palma). Comité Oceanográfico Nacional–Pontificia Universidad Católica de Valparaíso, Valparaíso, Chile, pp. 53–58.
- Silva N. and Prego R. (2002) Carbon and nitrogen spatial segregation and stoichiometry in the surface sediments of southern Chilean inlets (41–56°S). *Estuar. Coast. Shelf Sci.* **55**, 763–775.
- Silva N. and Guzman D. (2006) Condiciones oceanográficas físicas y químicas, entre Boca del Guafo y Fiordo Aysén (Crucero Cimar 7 Fiordos). *Cienc. Tecnol. Mar.* **29**(1), 25–44.
- Silva N., Vargas C. A. and Prego R. (2011) Land-ocean distribution of allocthonous organic matter in the surface sediments of the Chiloé and Aysén interior seas (Chilean Northern Patagonia). *Cont. Shelf Res* **31**(3–4), 330–339.
- Stern C., Moreno H., López-Escobar L., Clavero J., Lara L., Naranjo J., Parada M. and Skewes M. (2007) Chilean volcanoes. In *The geology of Chile* (eds T. Moreno and W. Gibbons). Geological Society of London, Bath, pp. 147–178.

- Strub P. T., Mesias J. M., Montecino V., Ruttlant J. and Salinas S. (1998) Coastal ocean circulation off Western South America. In *The Global Coastal Ocean. Regional Studies and Syntheses* (eds. A. R. Robinson and K. H. Brink). Wiley, New York, pp. 273–315.
- Toggweiler J. R. (2009) Shifting westerlies. *Science* **323**, 1434–1435.
- Tjallingii R., Rohl U., Kolling M. and Bickert, T. (2007) Influence of the water content on X-ray fluorescence core-scanning measurements in soft marine sediments. *Geochem. Geophys. Geosyst.* **8**, Q02004. doi:10.1029/2006GC001393.
- Van der Weijden C. H. (2002) Pitfalls of normalization of marine geochemical data using a common divisor. *Mar. Geol.* **184**, 167–187.
- Verardo D., Froelich P. and McIntyre A. (1990) Determination of organic carbon and nitrogen in marine sediments using the Carlo Erba NA-1500 analyzer. *Deep Sea Res. Part A* **37**, 157–165.
- Verhoogen J. (1962) Distribution of titanium between silicates and oxides in igneous rocks. *Am. J. Sci.* **260**, 211–220.
- Villalba R., Boninsegna J. A., Veblen T. T., Schmelter A. and Rubulis S. (1997) Recent trends in tree-ring records from high elevation sites in the Andes of northern Patagonia. *Clim. Change* **36**, 425–454.
- Villalba R., Grosjean M. and Kiefer T. (2009) Long-term multiproxy climate reconstructions and dynamics in South America (LOTRED-SA): state of the art and perspectives. *Palaeogeogr. Palaeoclimatol. Palaeoecol.* **281**, 175–179.
- Waldmann N., Ariztegui D., Anselmetti F. S., Austin J. J. A., Moy C. M., Stern C., Recasens C. and Dunbar R. (2010) Holocene Climatic Fluctuations and Positioning of the Southern Hemisphere Westerlies in Tierra del Fuego (54°S), Patagonia. *J. Quat. Sci.* doi:10.1002/jqs.1263.
- White A. F. and Blum A. E. (1995) Effects of climate on chemical weathering in watersheds. *Geochim. Cosmochim. Acta* **59**, 1729–1747.

Associate editor: Sidney R. Hemming